# NASA Technical Memorandum 74092

(NASA-TM-74092) SUBSONIC LONGITUDINAL AND LATERAL-DIRECTIONAL STATIC AERODYNAMIC CHARACTERISTICS FOR A CLOSE-COUPLED WING-CANARD MODEL IN BOTH SWEPT BACK AND SWEPT FORWARD CONFIGURATIONS (NASA) 60 p HC G3/02

N78-21049

Unclas
12374

SUBSONIC LONGITUDINAL AND LATERAL-DIRECTIONAL STATIC AERODYNAMIC CHARACTERISTICS FOR A CLOSE-COUPLED WING-CANARD MODEL IN BOTH SWEPT BACK AND SWEPT FORWARD CONFIGURATIONS

Jarrett K. Huffman and Charles H. Fox, Jr.

1978



National Aeronautics and Space Administration

Langley Research Center
Hampton, Virginia 23665

ABSTRACT

A general research fighter model was tested in the Langley 7- by 10-foot high speed tunnel at a Mach number of 0.3. The close-coupled wing-canard combination was tested with both lifting surfaces in a 60° swept back configuration and in a 32° swept forward configuration. The angle of attack range was from approximately -4° to 48° at sideslip angles of 0°, -5°, and 5°. The data are presented without analysis in order to expedite publication.

# INTRODUCTION

In the late 1940's, as aircraft speeds were approaching Mach one, investigations were conducted to evaluate swept forward and swept back wings as a means of delaying the onset of transonic compressibility effects. (See references 1-3). Sweeping the wings, either forward or back, delayed the drag rise to a higher Mach number; however, an aeroelastic divergence problem was found to be associated with swept forward wings. (See references 4 and 5.) This structural instability problem could be eliminated, but the resulting swept forward wing was significantly heavier than a corresponding swept back wing. As a consequence of this fact, most of the subsequent research was concentrated on swept back wings.

Recently, research interest in forward sweep has been renewed. This is partly a result of studies, such as reference 6, which indicate that proper tailoring of composite materials can produce a swept forward wing with minimal weight penalty. Forward sweep is being studied in relation to a variety of configurations. When applied to fighter aircraft, the forward sweep concept offers the potential for improved subsonic and supersonic cruise performance as well as improved transonic maneuver performance.

Experimental studies have been initiated to expand the existing data base on swept forward wings. (See reference 7.) The present study was conducted to obtain the static aerodynamic characteristics of a close coupled wing-canard model with both swept back and swept forward wing and canard surfaces.

It should be noted that the models were built up from wing and canard model parts previously constructed for swept back configurations. These lifting surfaces had circular arc airfoil sections which allowed their use in the reversed or forward sweep condition. It should be also noted that, because of the flow separation at the sharp leading edges, the present data will be generally more applicable to the study of the high angle-of-attack characteristics.

The tests were performed in the Langley 7- by 10-foot high speed tunnel at a Mach number of 0.3. The angle-of-attack range was from approximately $-4^\circ$ to $48^\circ$ at sideslip angles of $0^\circ$, $-5^\circ$, and $5^\circ$.

## SYMBOLS

The International System of Units, with the U.S. Customary Units presented in parenthesis, is used for the physical quantities in this report (See reference 8). The measurements and calculations were made in the U.S. Customary Units. The data presented in this report are referred to the stability axis system. The reference center for moments is shown in Figure 1(a).

$b$ wing reference span, .508 m (20.000 in.)

$\bar{c}$ wing reference chord, .233 m (9.185 in.)

$C_D$ total drag coefficient, $\frac{\text{Drag}}{qS}$

$C_{D_2}$ nose drag coefficient

$C_L$ total lift coefficient, $\frac{\text{Lift}}{qS}$

$C_{L_2}$ nose lift coefficient

$C_\ell$ total rolling moment coefficient, $\frac{\text{Rolling moment}}{qSb}$

$C_{\ell_2}$ nose rolling moment coefficient

$C_{\ell_\beta}$ beta derivative of total rolling moment coefficient computed between $\beta = 5°$ and $\beta = -5°$.

$C_{\ell_{\beta_2}}$ beta derivative of nose rolling moment coefficient computed between $\beta = 5°$ and $\beta = -5°$

$C_m$ total pitching moment coefficient, $\frac{\text{Pitching moment}}{qS\bar{c}}$

$C_{m_2}$ nose pitching moment coefficient

$C_n$ total yawing moment coefficient, $\frac{\text{Yawing moment}}{qSb}$

$C_{n_2}$ nose yawing moment coefficient

$C_{n_\beta}$ beta derivative of total yawing moment coefficient computed between $\beta = 5^\circ$ and $\beta = -5^\circ$

$C_{n_{\beta_2}}$ beta derivative of nose yawing moment coefficient computed between $\beta = 5^\circ$ and $\beta = -5^\circ$

$C_Y$ total side force coefficient, $\frac{\text{Side force}}{qS}$

$C_{Y_2}$ nose side force coefficient

$C_{Y_\beta}$ beta derivative of total side force coefficient computed between $\beta = 5^\circ$ and $\beta =-5^\circ$

$C_{Y_{\beta_2}}$ beta derivative of nose side force coefficient computed between $\beta = 5^\circ$ and $\beta = -5^\circ$

M free stream Mach number

q free stream dynamic pressure, Pa ($lb/ft^2$)

S wing reference area, .1032 $m^2$ (1.11109 $ft^2$)

$\alpha$ angle of attack of the model, degrees

$\alpha_2$ angle of attack of the fuselage nose, degrees

$\beta$ angle of sideslip of the model, degrees

$\beta_2$ angle of sideslip of the fuselage nose, degrees

$\Lambda_w$ leading edge sweep angle of the wing, degrees

$\Lambda_c$ leading edge sweep angle of the canard, degrees

Model

B body

C canard

V vertical tail

W wing

## DESCRIPTION OF MODEL

Drawings of the model tested are presented in Figure 1. Photographs of the model installed in the 7- by 10-foot high speed tunnel are presented in Figure 2. The basic model consisted of a main fuselage with a vertical tail and a wing and a fuselage nose with a canard. The main fuselage was sting mounted on a six-component strain gage main balance which measured the total forces and moments on the configuration. The fuselage nose section was mounted on a six component strain gage nose balance which measured only the forces and moments on the nose and canard. The metric break is shown in figure 1.

The uncambered and untwisted wing, canard and vertical tail employed circular arc airfoil sections with a thickness ratio of 6% at the fuselage juncture and 4% at the tip. The wing and canard had one edge with a nominal sweep of 60° and one edge with a nominal sweep of 32° (See Figures 1(a) - 1(d)). The wing and canard could be set up with the leading edge swept back 60° or with the leading edge swept forward 32°. The exposed area of the canard was 15.9 percent of the wing reference area. The centerline mounted vertical tail, which is shown in Figure 1(e), had an exposed area of 14 percent of the wing reference area.

## APPARATUS, TESTS, AND CORRECTIONS

The investigation was conducted in the Langley 7- by 10-foot high speed tunnel (See reference 9). Forces and moments were measured on two six component strain gage balances mounted internally in the model. The test was run at a Mach number of 0.3 corresponding to a Reynolds number of $1.4 \times 10^6$ based on the wing reference chord. The model was tested over an angle of attack range from -4° to approximately 48° at sideslip angles of 0°, and ±5°. The angles of attack and sideslip have been corrected for the effects of sting and balance bending under load. It should be noted that the sting support system which permits testing over this large angle range is designed specifically for stability testing. Therefore the level of the drag data is questionable for use in performance analysis.

Jet boundary and blockage corrections have been applied to the data based on references 10 and 11, respectively. The main balance chamber pressure was measured and the total drag measurements were adjusted to a condition of free stream static pressure acting over the base of the model. The nose balance base and chamber pressure were also measured and the nose drag measurements were adjusted to a condition of free stream static pressure acting at the base of the nose. Transition strips 0.16 cm (.0625 in.) in width of No. 120 Carborundum grams were placed 2.54 cm (1.0 in.) aft of the leading edge of the wings, canards, and vertical tail as well as 3.05 cm (1.2 in.) aft of the nose of the fuselage (reference 12).

## PRESENTATION OF RESULTS

The results are presented without analysis in order to expedite publication. Figure 3 presents surface oil flow photographs.

The longitudinal and lateral-directional aerodynamic characteristics at 0° sideslip are presented in the following figures:

| | Figure |
|---|---|
| Swept back configuration: | |
| Vertical tail on | 4 |
| Vertical tail off | 5 |
| Swept forward configuration: | |
| Vertical tail on | 6 |
| Vertical tail off | 7 |

The lateral-directional aerodynamic stability derivative characteristics are presented in the following figures:

| | |
|---|---|
| Swept back configuration: | |
| Vertical tail on | 8 |
| Vertical tail off | 9 |
| Swept forward configuration: | |
| Vertical tail on | 10 |
| Vertical tail off | 11 |

## REFERENCES


1. Wright, J. B., and Loving, D. L., High Speed Wind Tunnel Tests of 1/16-Scale Model of the D-558 Research Airplane, NACA RM L6J09 1947.
2. Whitcomb, R. T., An Experimental Study at Moderate and High Subsonic Speeds of the Flow over Wings with 30° and 45° of Sweep-Forward in Conjunction with a Fuselage, NACA RM L50K28, 1950.
3. Whitcomb, R. T., An Experimental Study at Moderate and High Subsonic Speeds of the Flow over Wings with 30° and 45° of Sweep-Back in Conjunction with a Fuselage, NACA RM L50K27, 1951.
4. Diederick, F. W.; and Budiansky, B.: Divergence of Swept Wings , ACA Technical Note 1680, 1948.
5. Bisplinghoff, R. L.; and Ashley, H.: Principles of Aeroelasticity, John Wiley and Sons, Inc., New York, 1962.
6. Krone, N. J., Lt. Col., Divergence Elimination with Advanced Composites, AIAA Paper No. 75-1009, Aircraft Systems and Technology Meeting, Los Angeles, California, August 1975.
7. Huffman, Jarrett K., and Fox, Charles H., Jr.: Subsonic Longitudinal and Lateral-Directional Static Aerodynamic Characteristics for a Model with Swept Back and Swept Forward Wings. NASA TM-74093, 1978.
8. Mechtly, E. A.: The International System of Units. NASA SP-7012, 1964.

9. Fox, Charles H., Jr., and Huffman, Jarrett K.: Calibration and Test Capabilities of the Langley 7- by 10-foot High Speed Tunnel. NASA TM X-74027, 1977.

10. Gillis, Clarence L.; Polhamus, Edward C., and Gray, Joseph L., Jr.: Charts for Determining Jet-Boundary Corrections for Complete Models in 7- by 10-foot Closed Rectangular Wing Tunnels. NACA WR-L-123, 1945.

11. Herriott, John G.: Blockage Corrections for Three-Dimensional-Flow Closed-Throat Wind Tunnels, with Consideration of the Effect of Compressibility. NACA Report 995, 1950.

12. Braslow, Albert L.; Hicks, Raymond M.; and Harris, Roy V., Jr.: Use of Grit-type Boundary-Layer Transition Trips on Wind Tunnel Models. NASA TN D-3579, 1966.

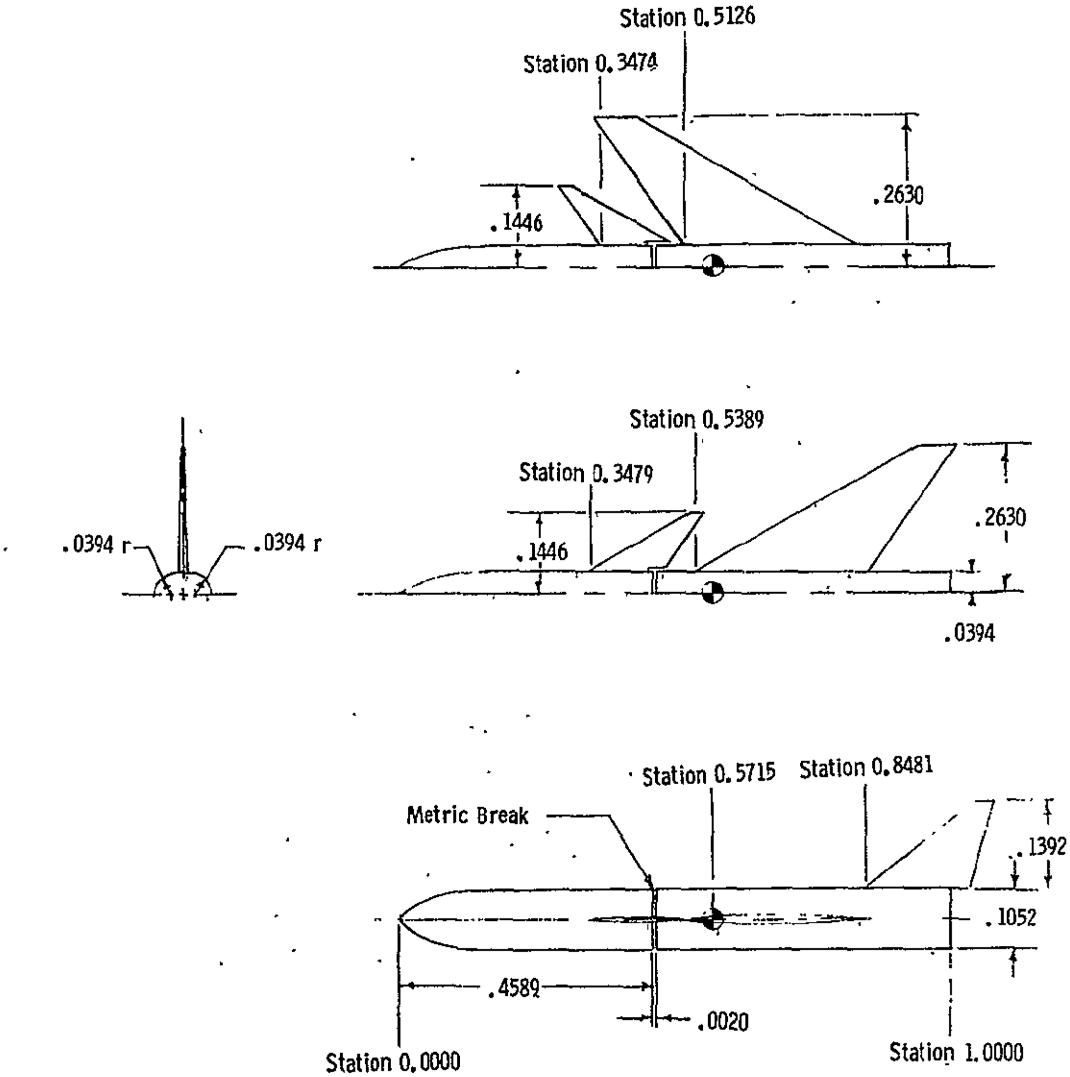


(a) General arrangement.

Figure 1. Drawings of the model tested. All dimensions are normalized by a fuselage length of 0.96589 m. (38.027 in.)

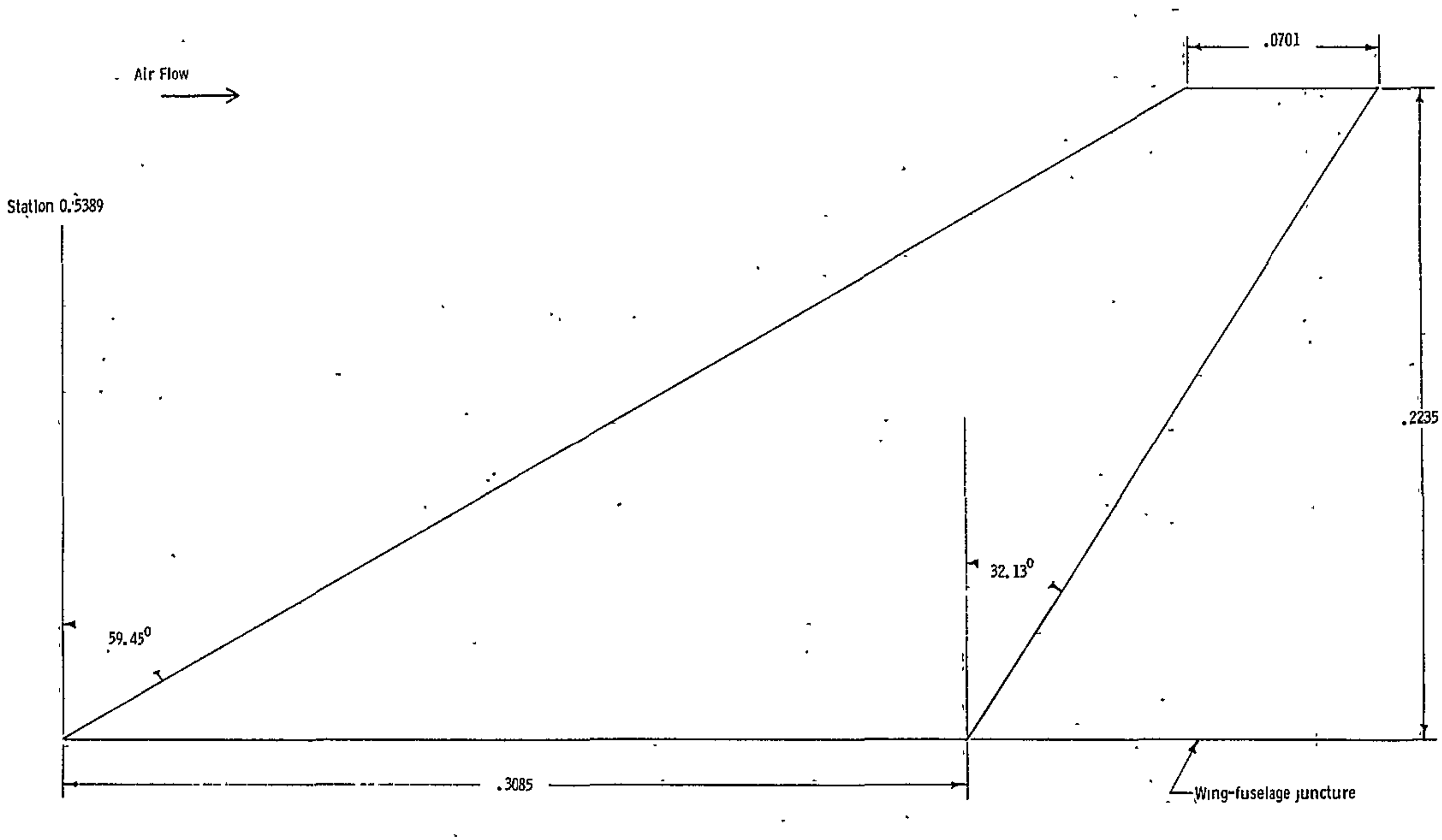


(b) Details of the swept back wing.

Figure 1. Continued.

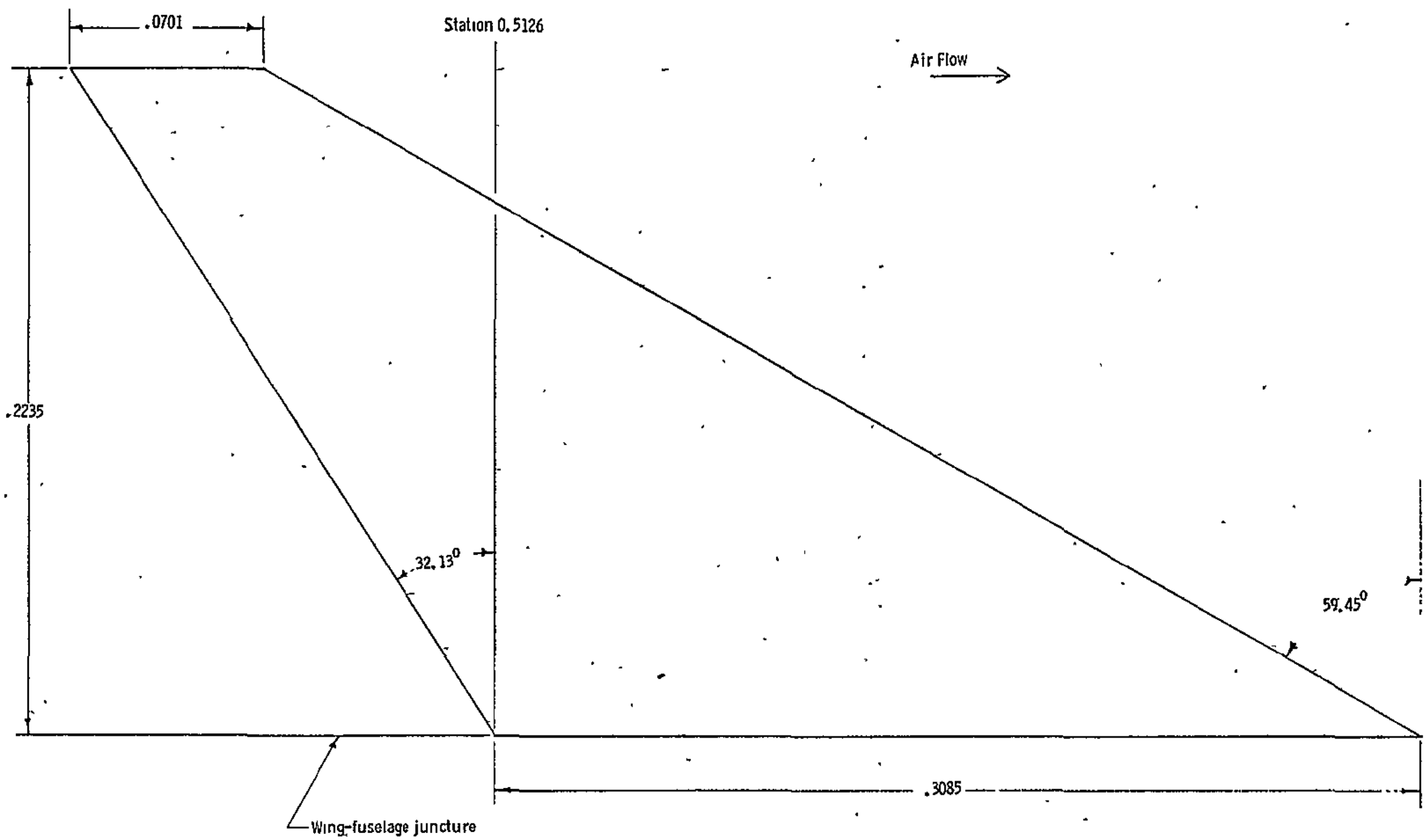


(c) Details of the swept forward wing.

Figure 1. Continued.

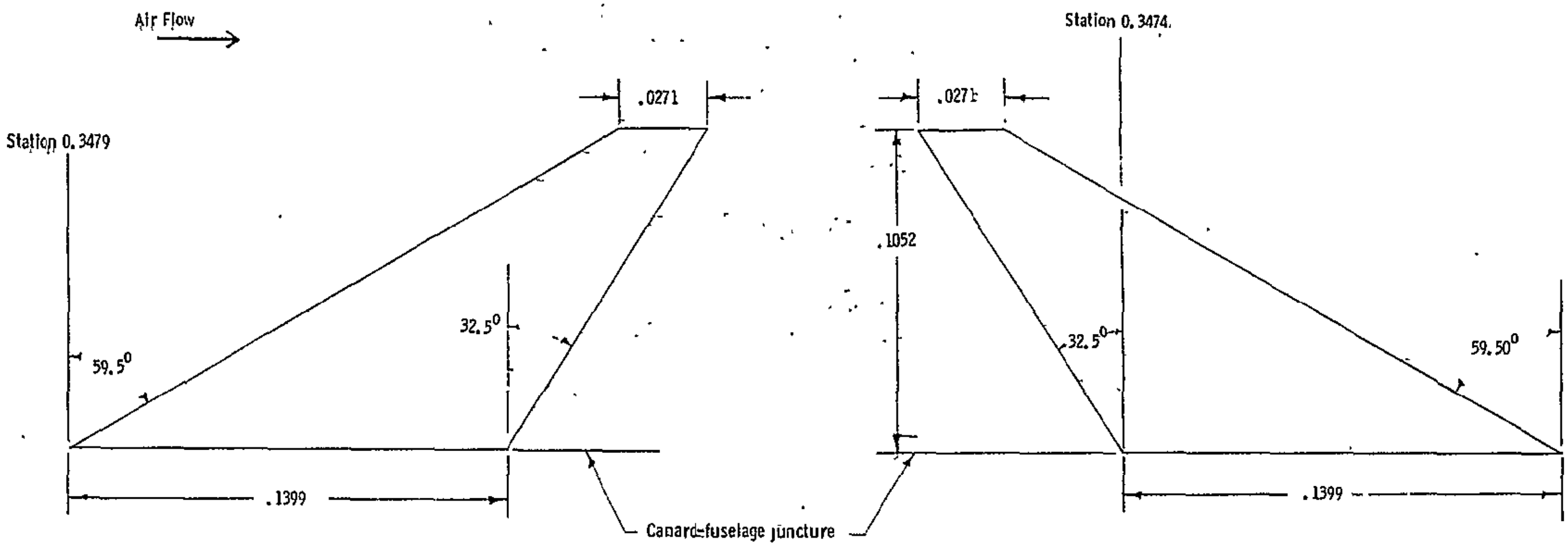


(d) Details of the swept back and swept forward canards.

Figure 1. Continued.

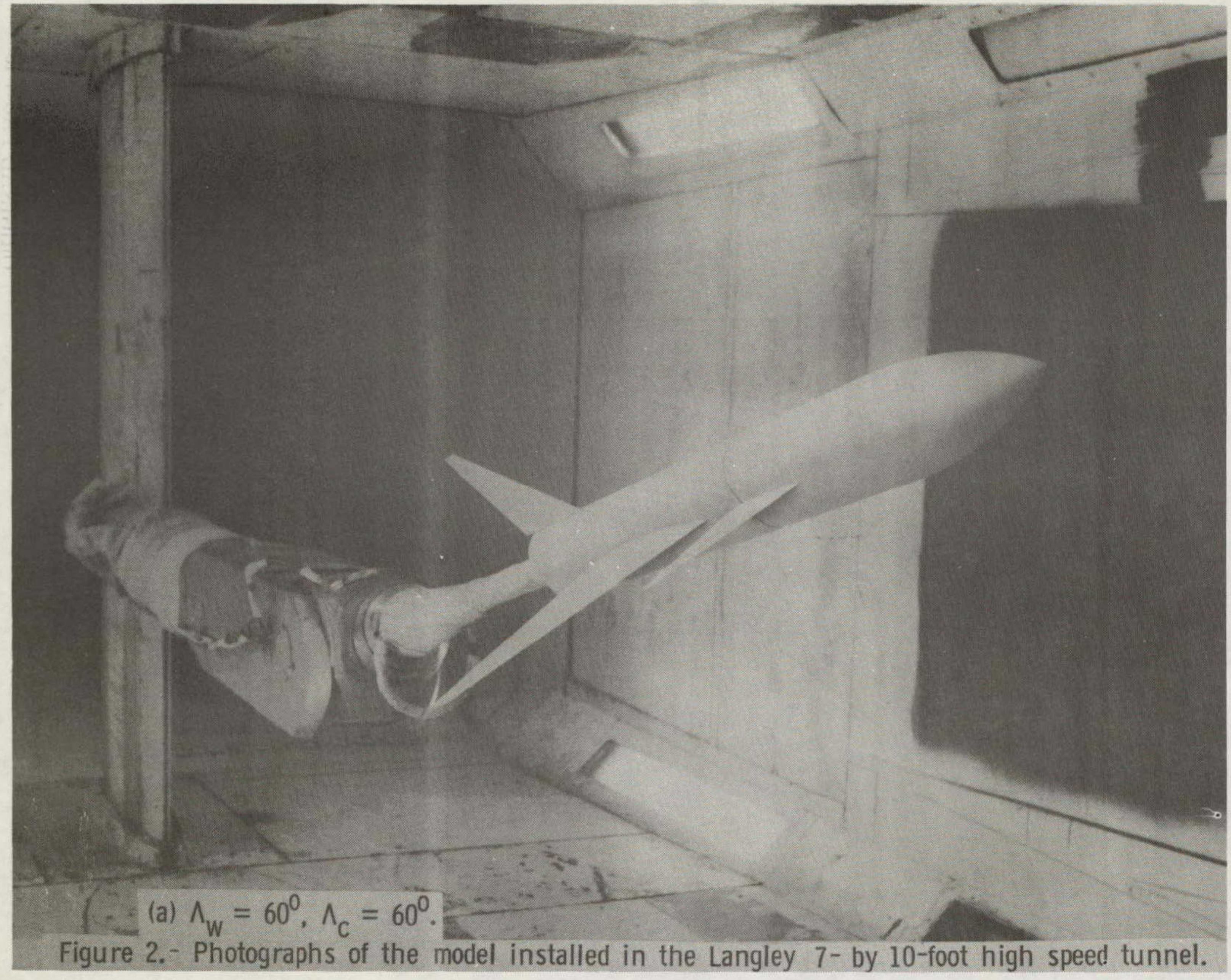

(a) $\Lambda_W = 60^0$, $\Lambda_C = 60^0$.

Figure 2.- Photographs of the model installed in the Langley 7- by 10-foot high speed tunnel.

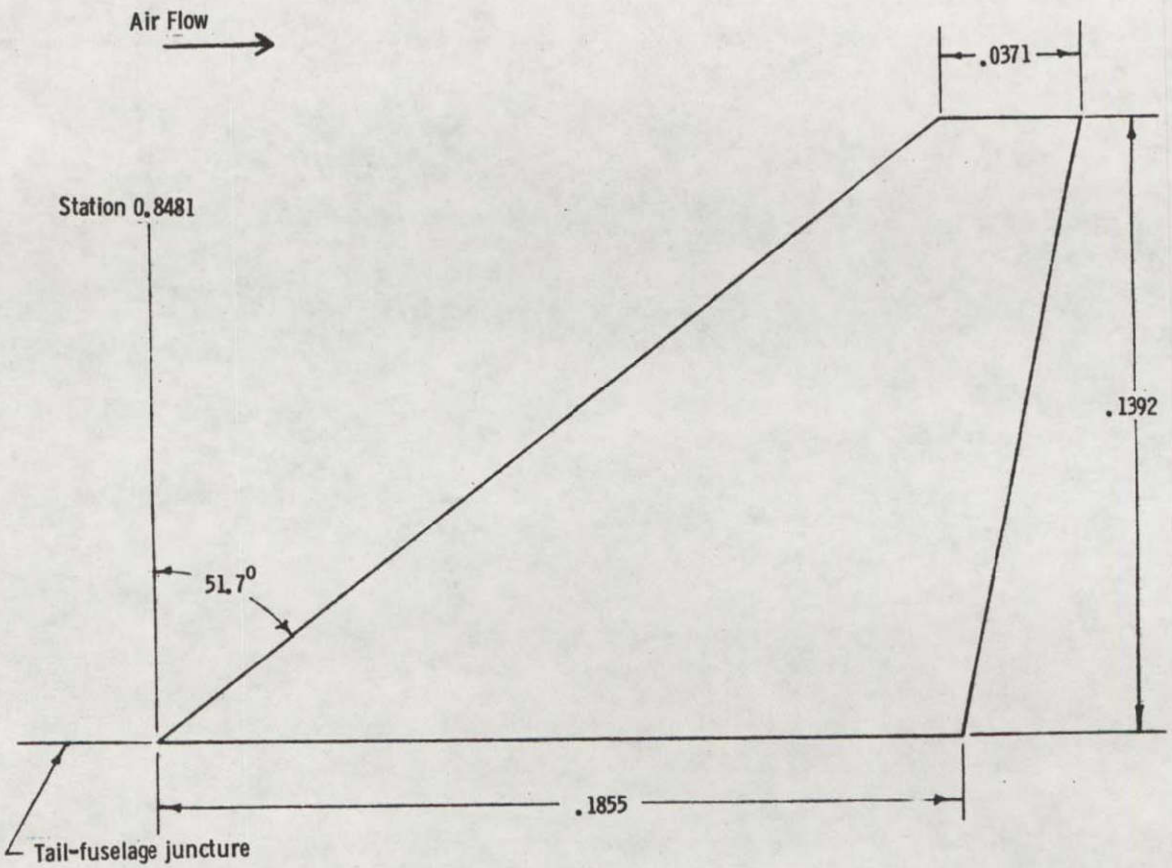


(e) Details of the vertical tail.

Figure 1. Concluded.

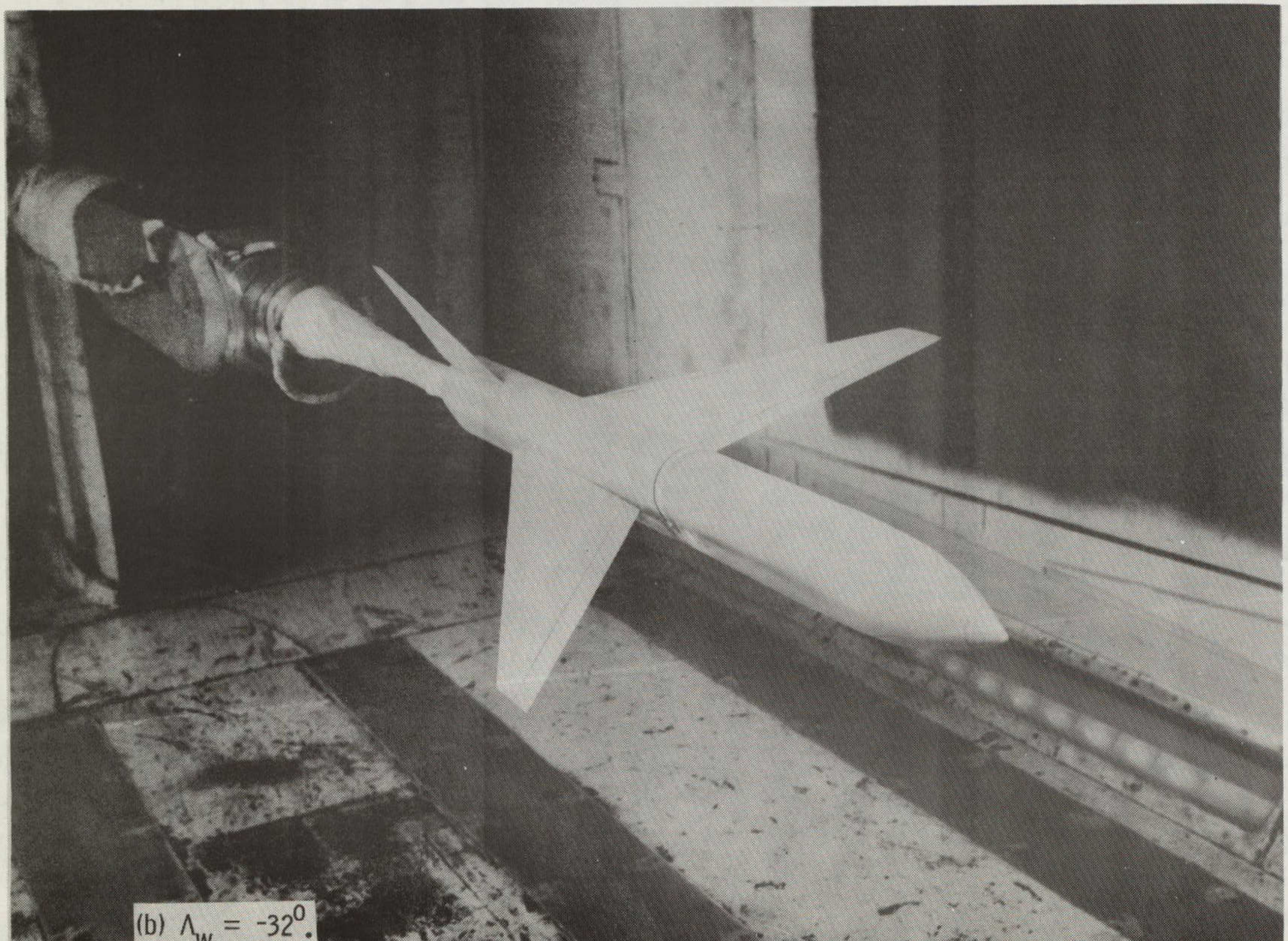

(b) $\Lambda_w = -32^o$.

Figure 2.- Continued.

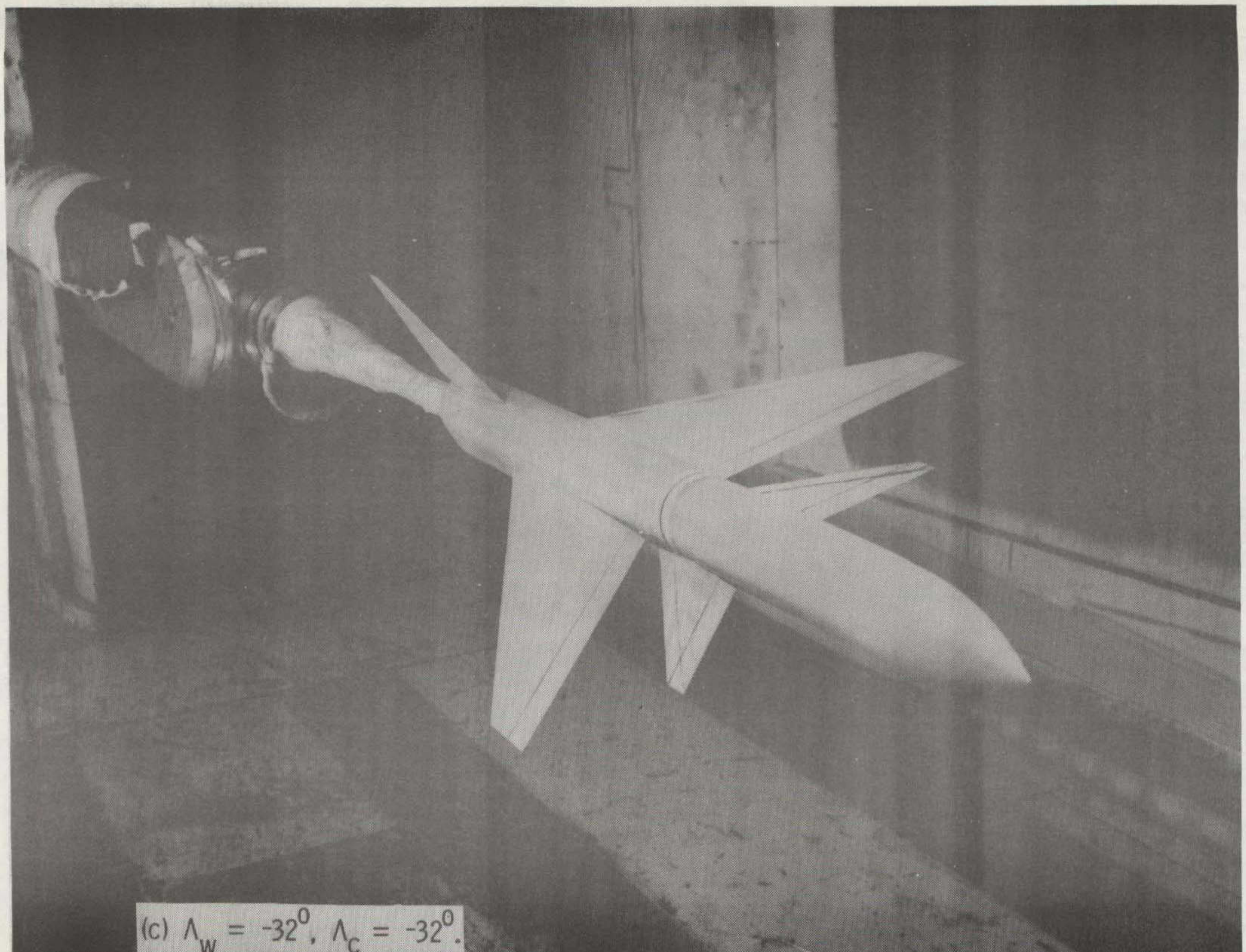

(c) $\Lambda_W = -32^0$, $\Lambda_C = -32^0$.

Figure 2.- Concluded.

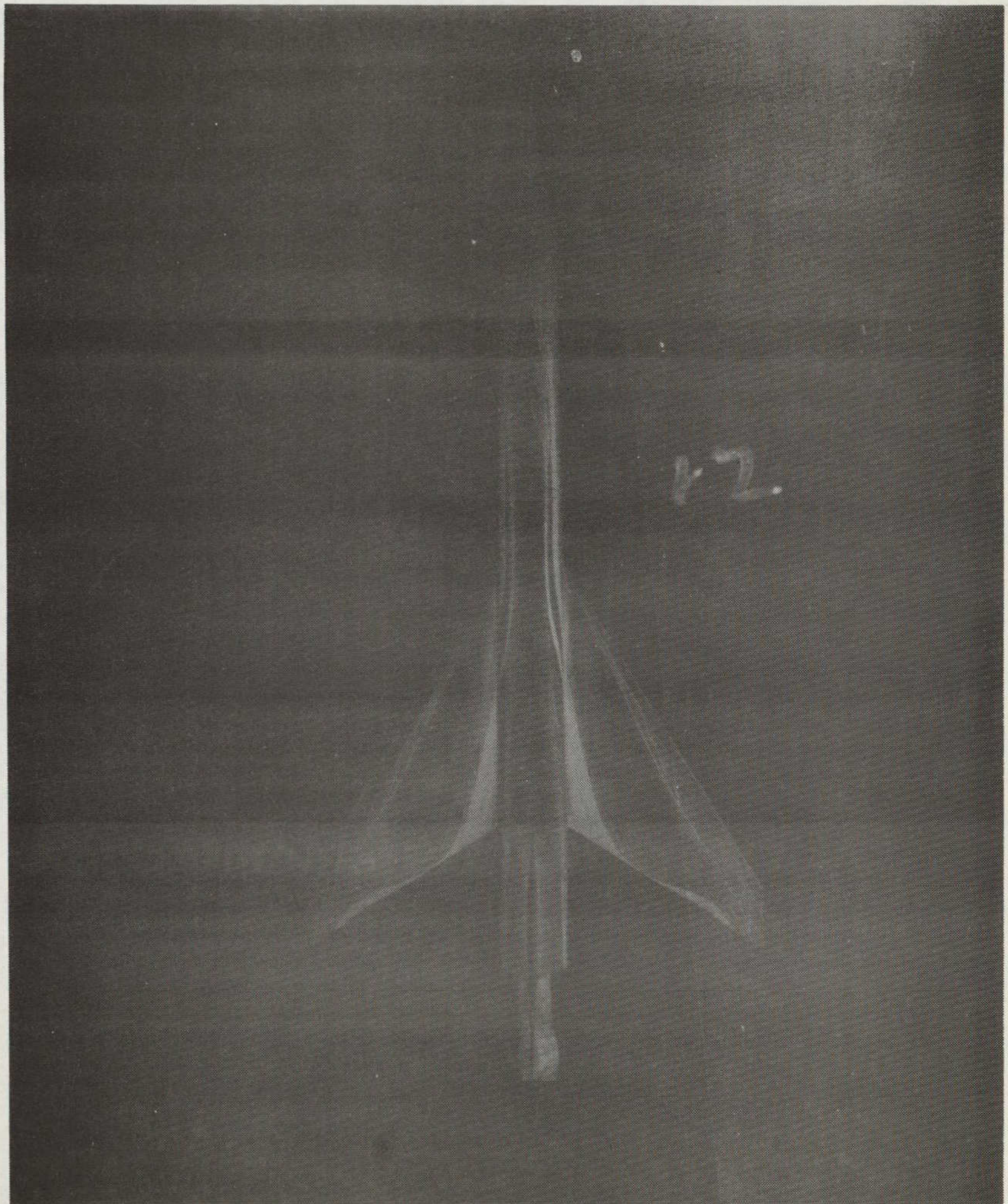

(a) $\alpha = 15^0$, $\Lambda_w = 60^0$, plan view.

Figure 3.- Surface oil flow photographs. M = 0.3.

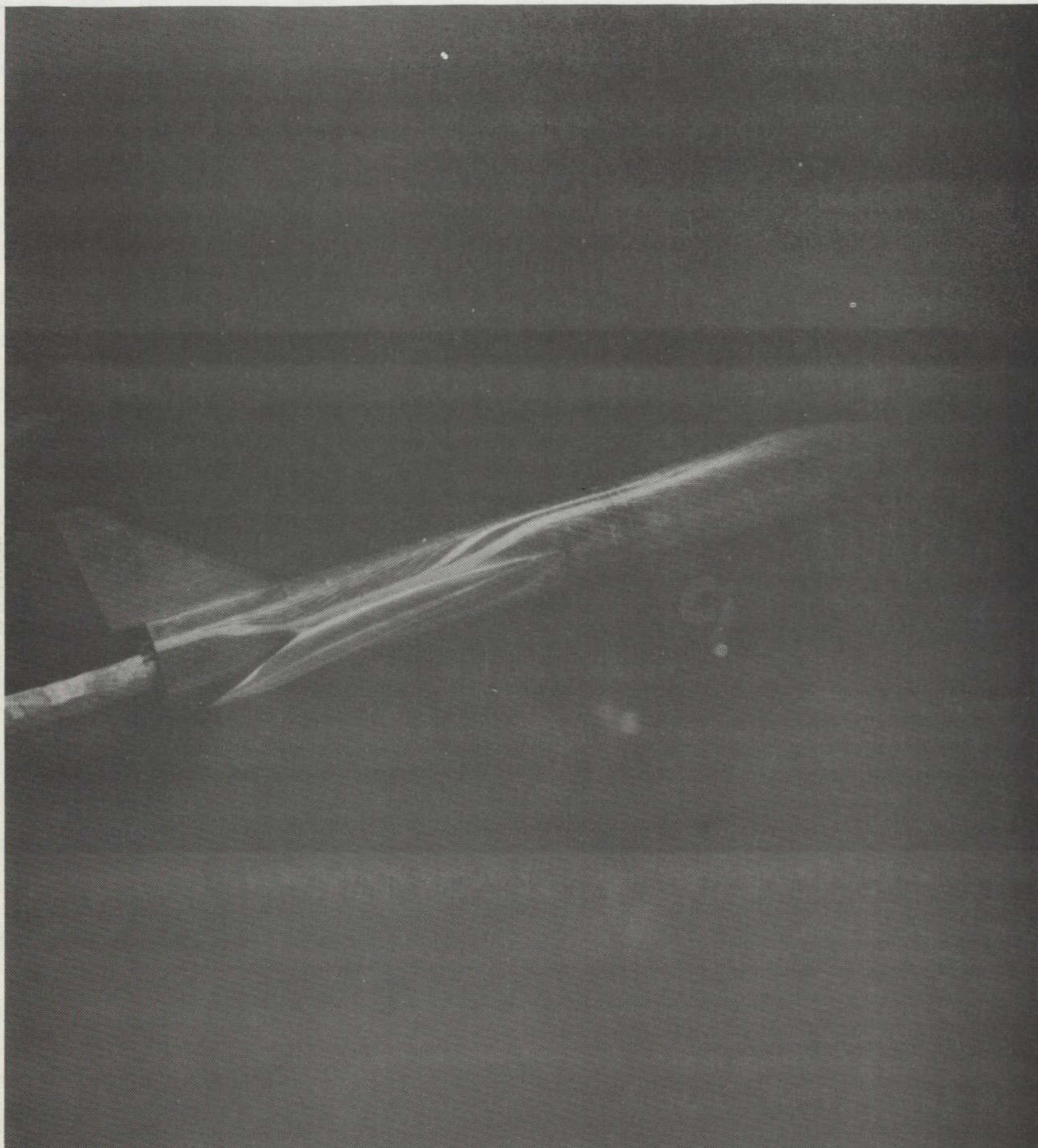

(b) $\alpha = 15^0$, $\Lambda_W = 60^0$, side view.

Figure 3.- Continued.

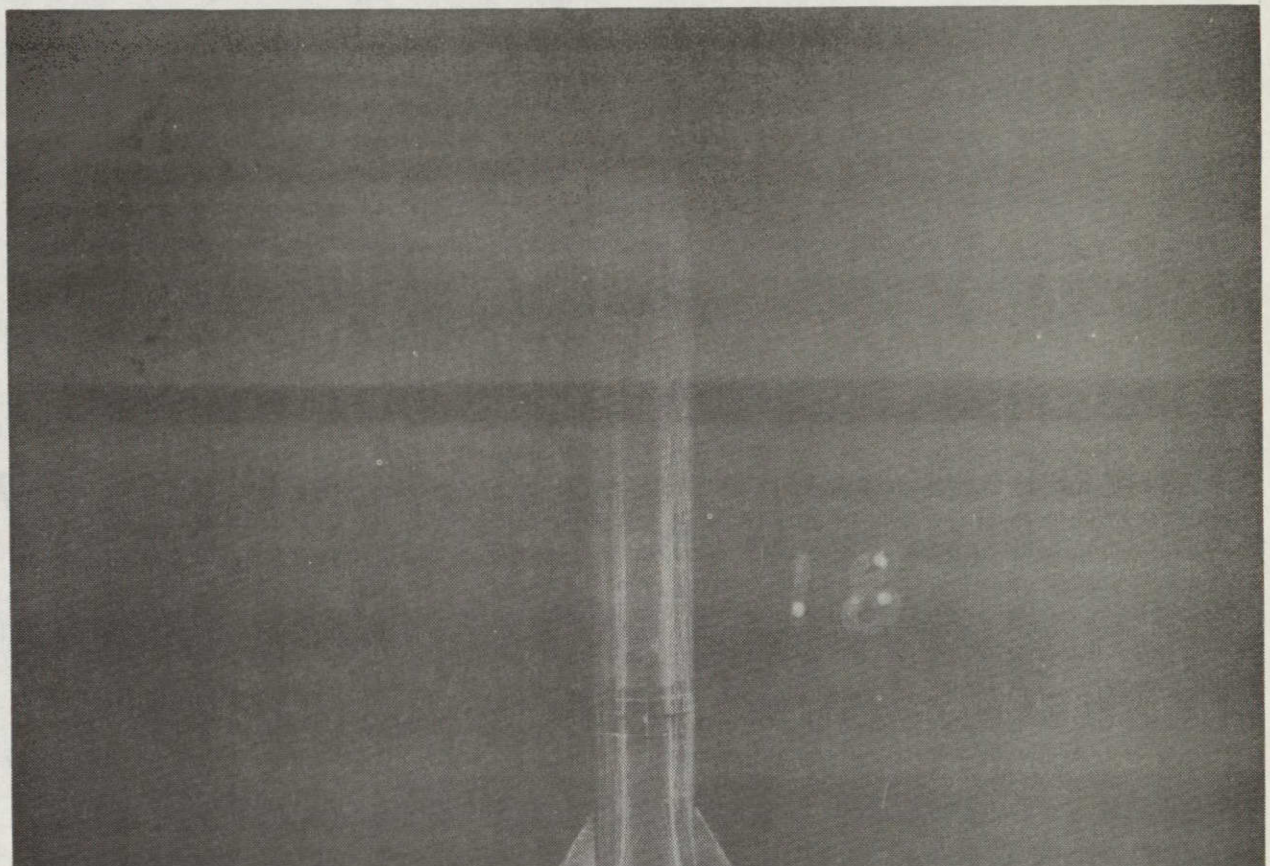

(c) $\alpha = 30^0$, $\Lambda_w = 60^0$, plan view.

Figure 3.- Continued.

ORIGINAL PAGE IS
OF POOR QUALITY

(d) $\alpha = 30^0$, $\Lambda_W = 60^0$, side view.

Figure 3.- Continued.

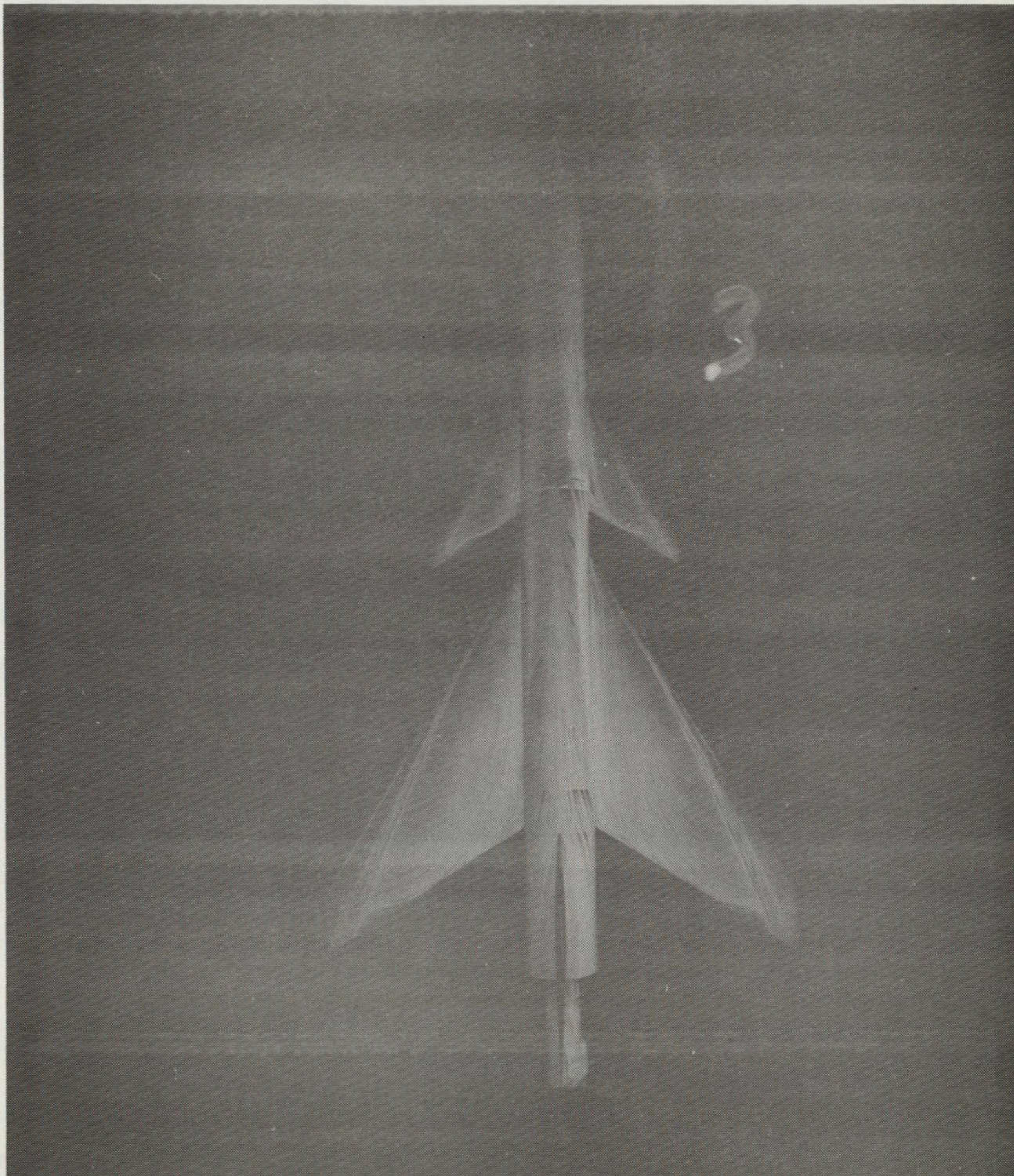

(e) $\alpha = 15^0$, $\Lambda_W = 60^0$, $\Lambda_c = 60^0$, plan view.

Figure 3.- Continued.

ORIGINAL PAGE IS
OF POOR QUALITY

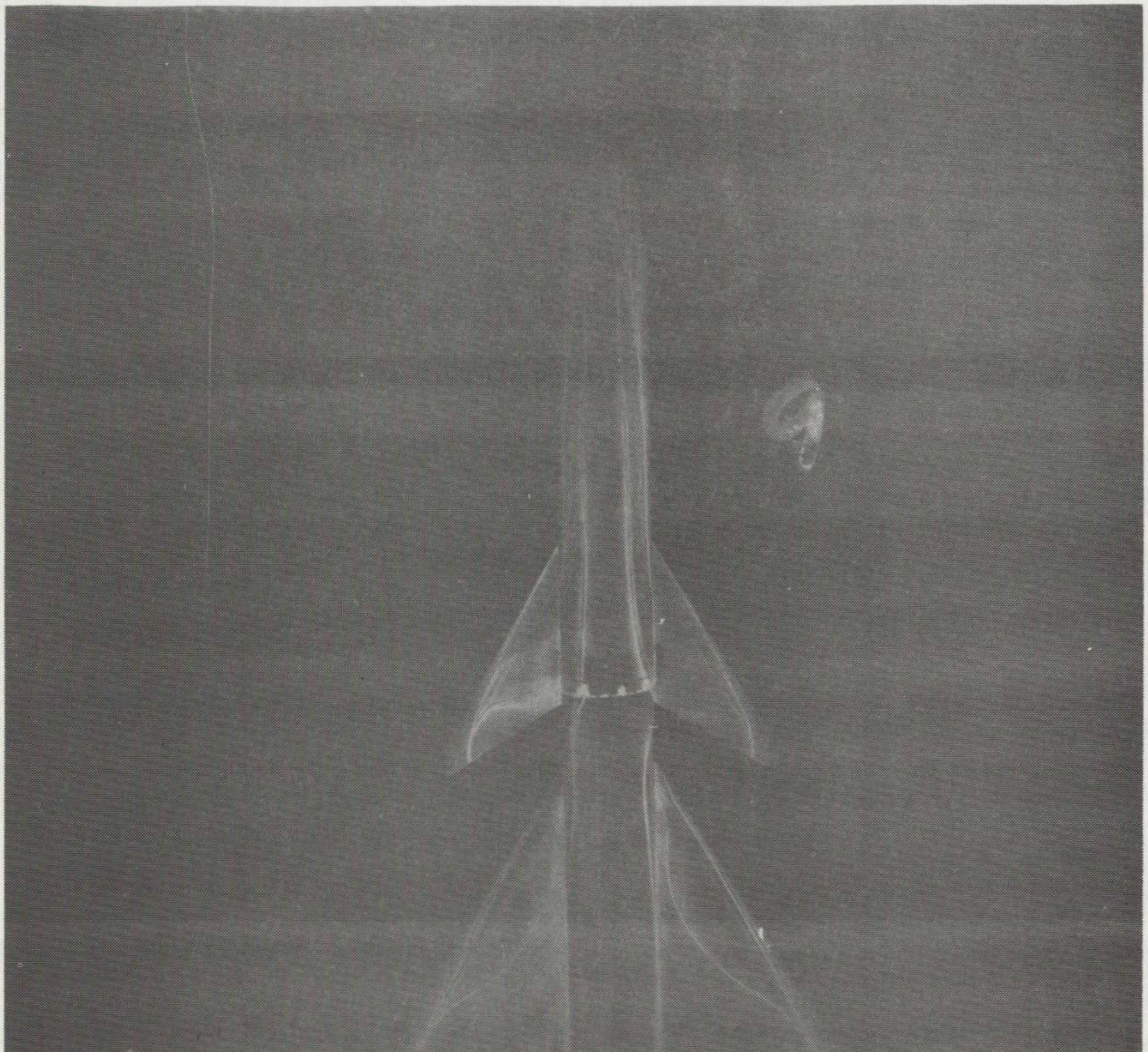

(f) $\alpha = 30^0$, $\Lambda_W = 60^0$, $\Lambda_c = 60^0$, plan view.

Figure 3.- Continued.

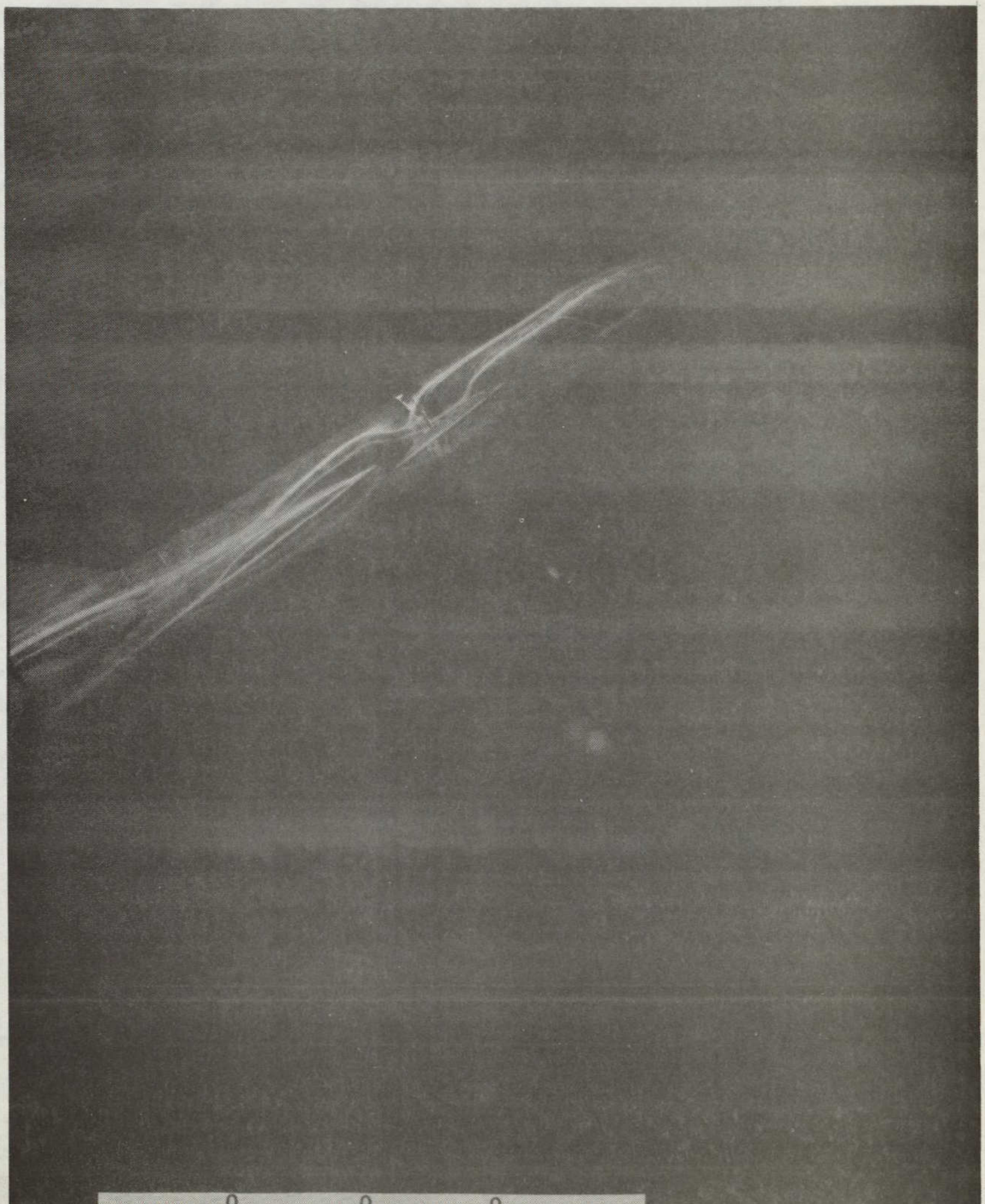

(g) $\alpha = 30^0$, $\Lambda_w = 60^0$, $\Lambda_c = 60^0$, side view.

Figure 3.- Continued.

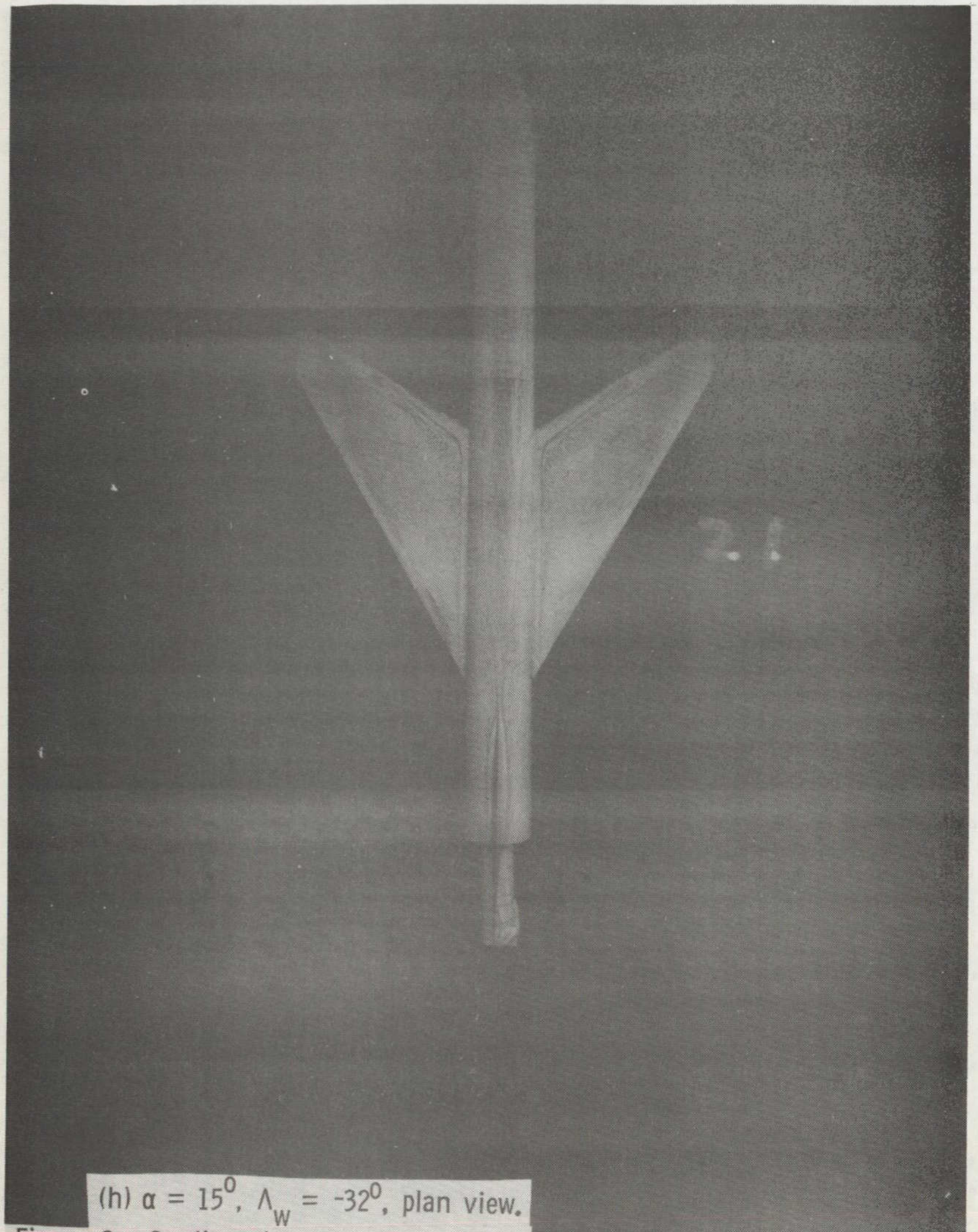


(h) $\alpha = 15^0$, $\Lambda_w = -32^0$, plan view.

Figure 3.- Continued.

(i) $\alpha = 15^0$, $\Lambda_W = -32^0$, side view.

Figure 3.- Continued.

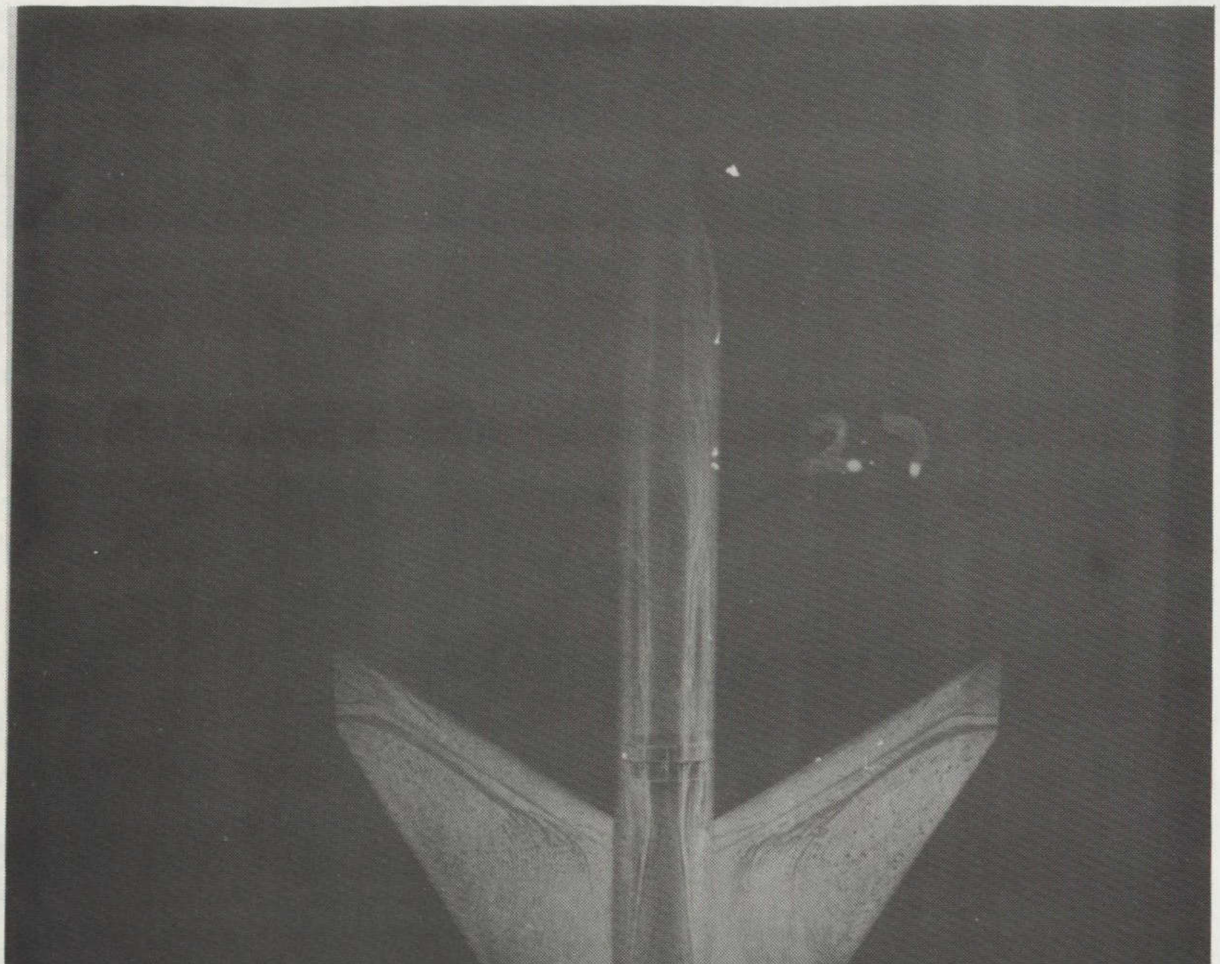


(j) $\alpha = 30^0$, $\Lambda_w = -32^0$, plan view.

Figure 3.- Continued.

(k) $\alpha = 30^0$, $\Lambda_w = -32^0$, side view.

Figure 3.- Continued.

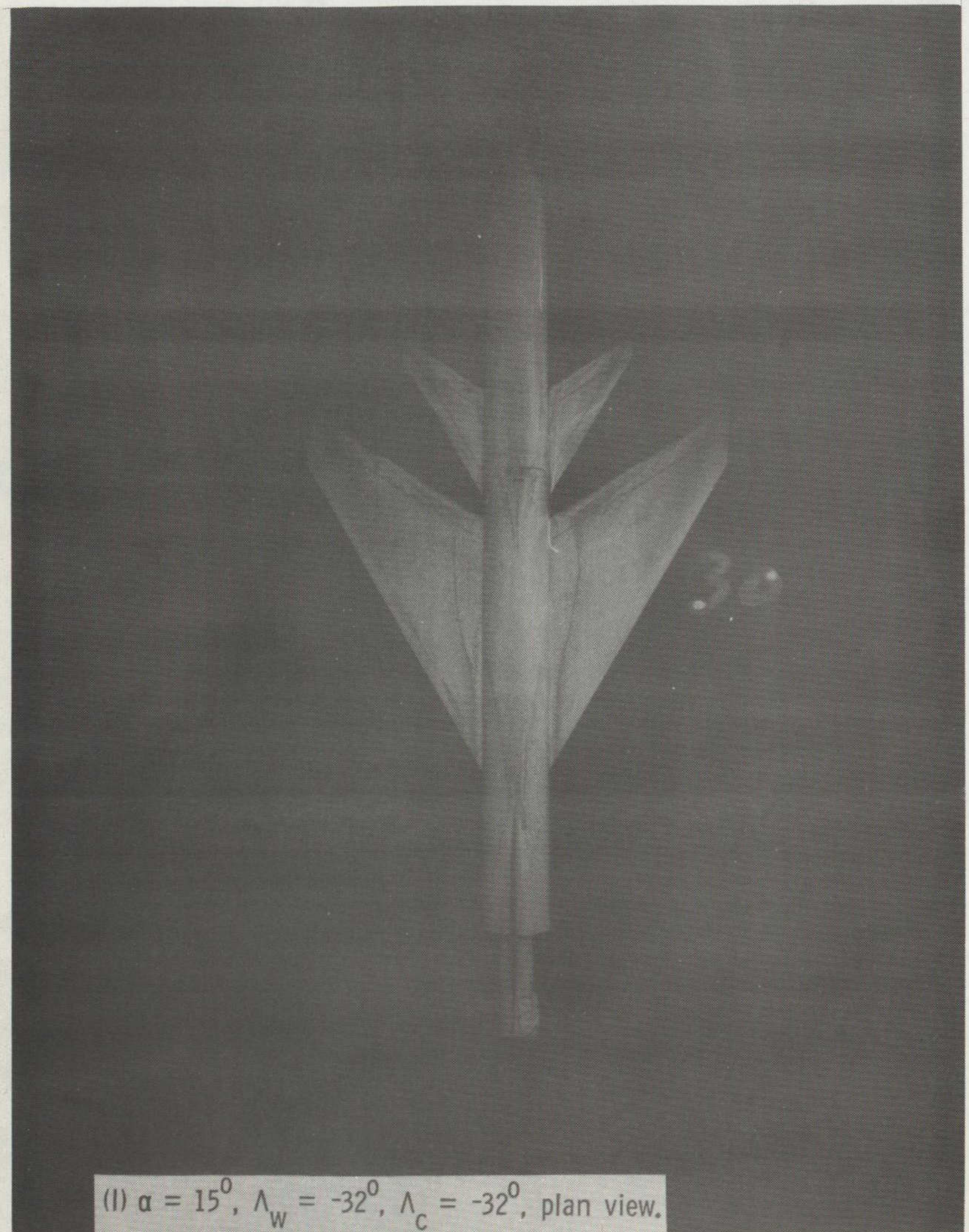

(l) $\alpha = 15^{0}$, $\Lambda_{W} = -32^{0}$, $\Lambda_{c} = -32^{0}$, plan view.

Figure 3.- Continued.

(m) $\alpha = 15^0$, $\Lambda_W = -32^0$, $\Lambda_c = -32^0$, side view.

Figure 3.- Continued.

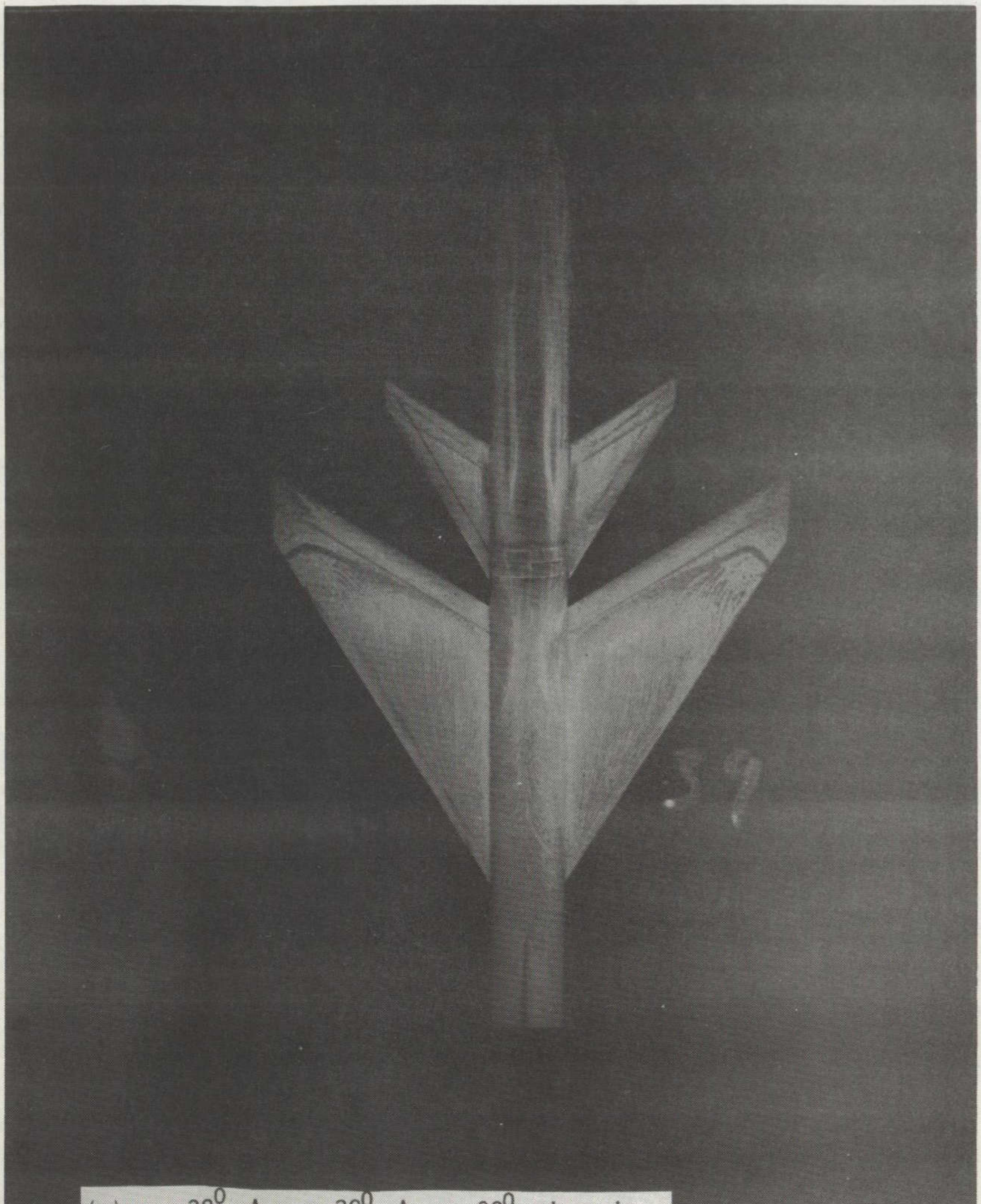

(n) $\alpha = 30^0$, $\Lambda_w = -32^0$, $\Lambda_c = -32^0$, plan view.

Figure 3.- Continued.

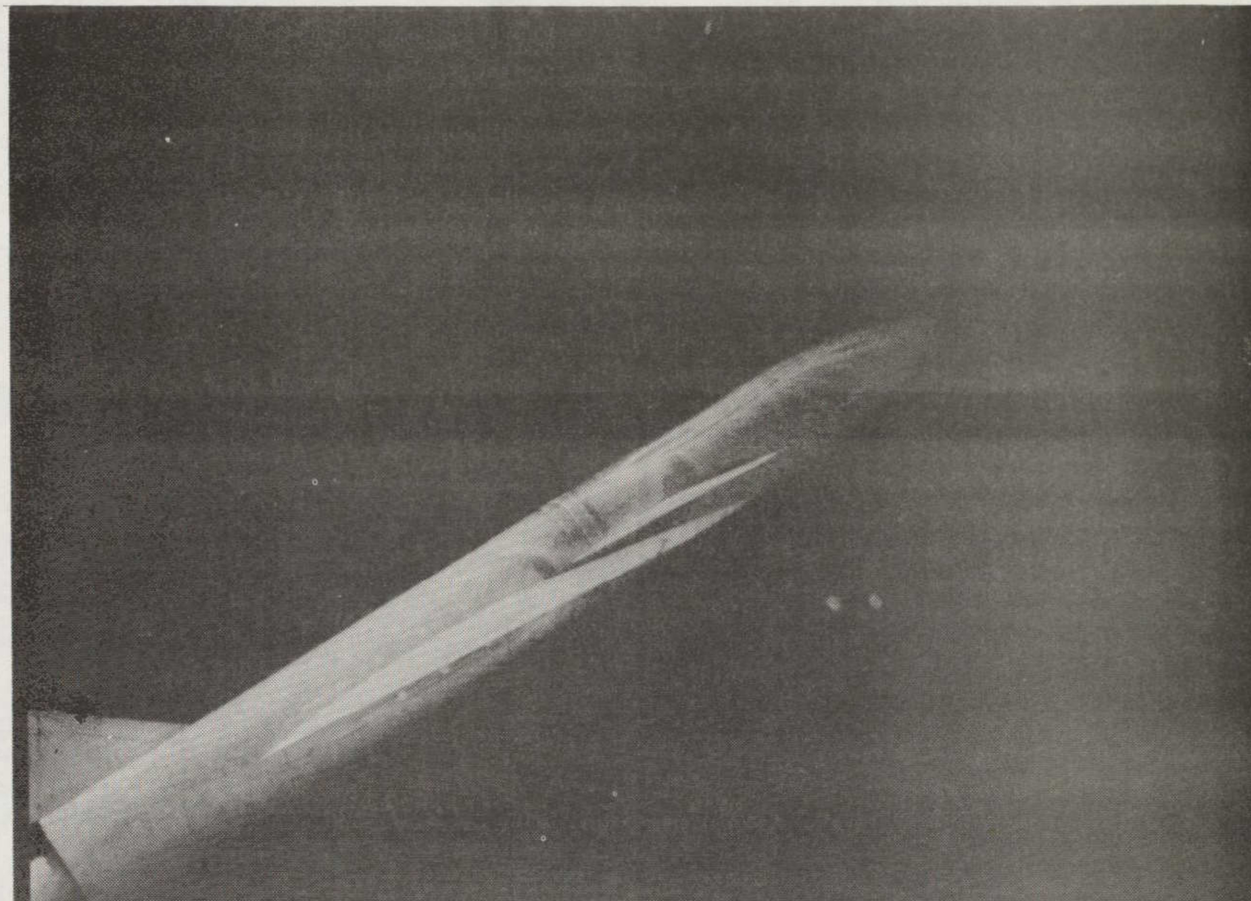

(o) $\alpha = 30^0$, $\Lambda_W = -32^0$, $\Lambda_c = -32^0$, side view.

Figure 3.- Concluded.

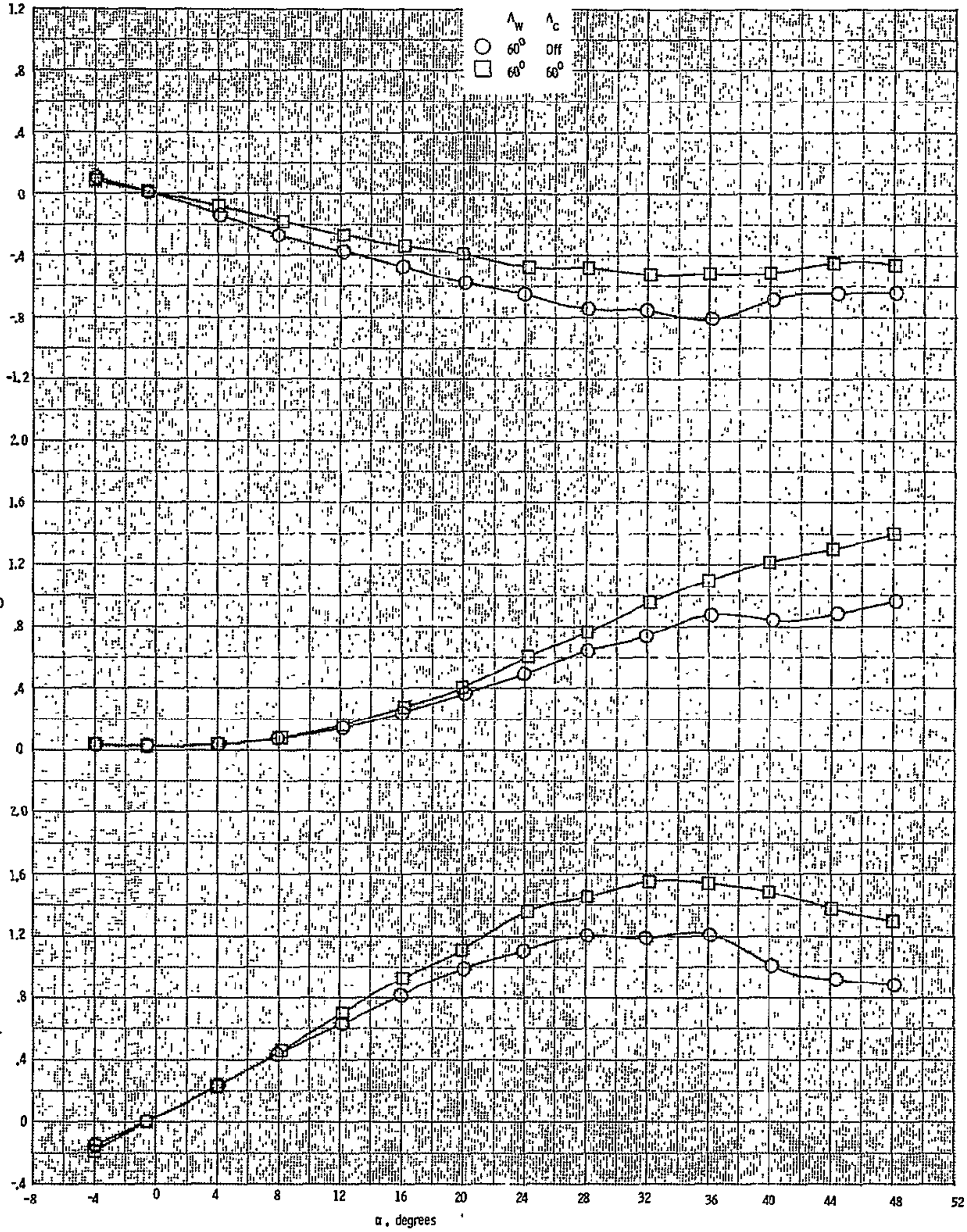


(a) Main balance longitudinal data

Figure 4. Aerodynamic characteristics of the swept back configuration with the vertical tail on. $M = 0.3$, $\beta = 0^\circ$.

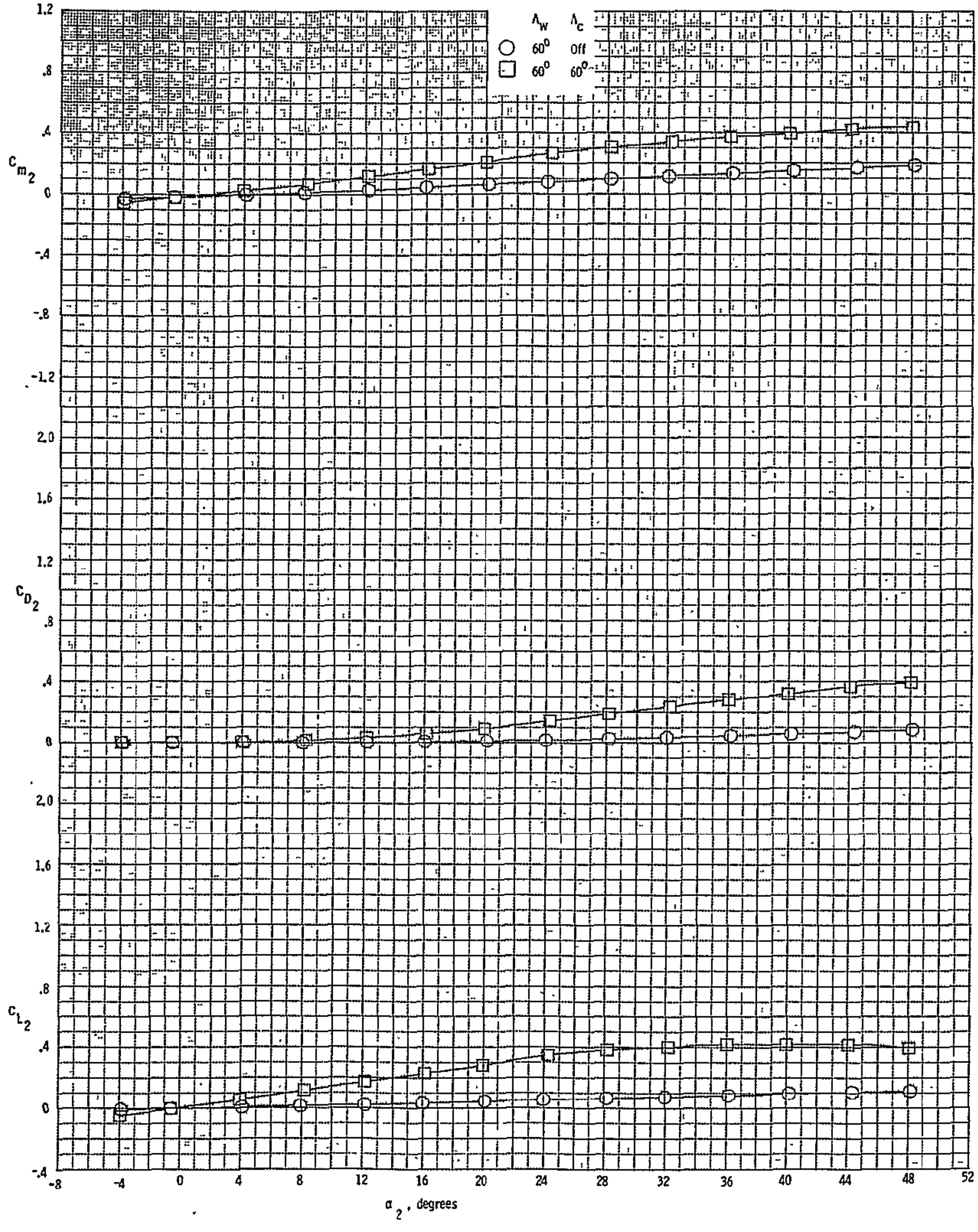


(b) Nose balance longitudinal data

Figure 4. Continued.

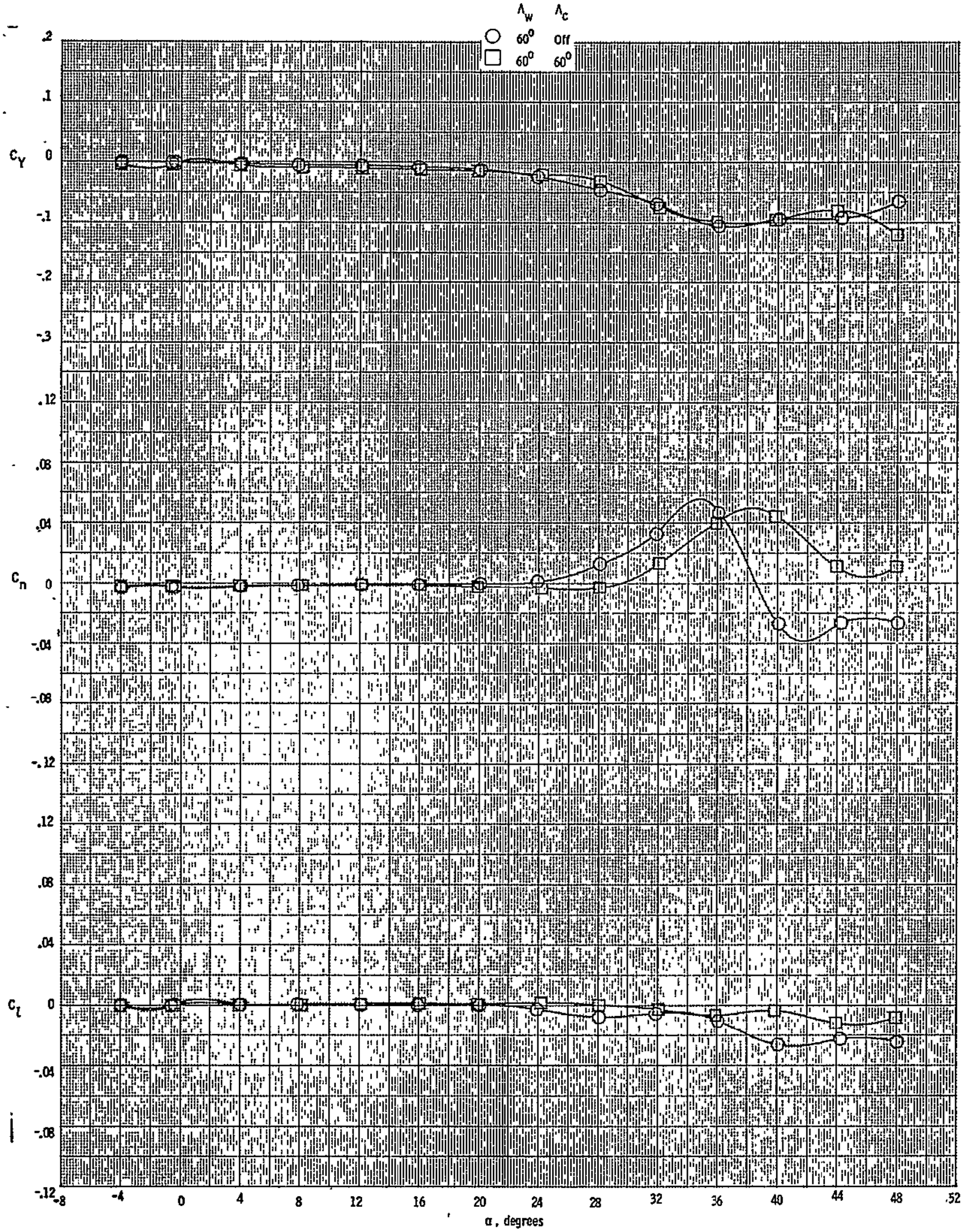


(c) Main balance lateral-directional data
Figure 4. Continued.

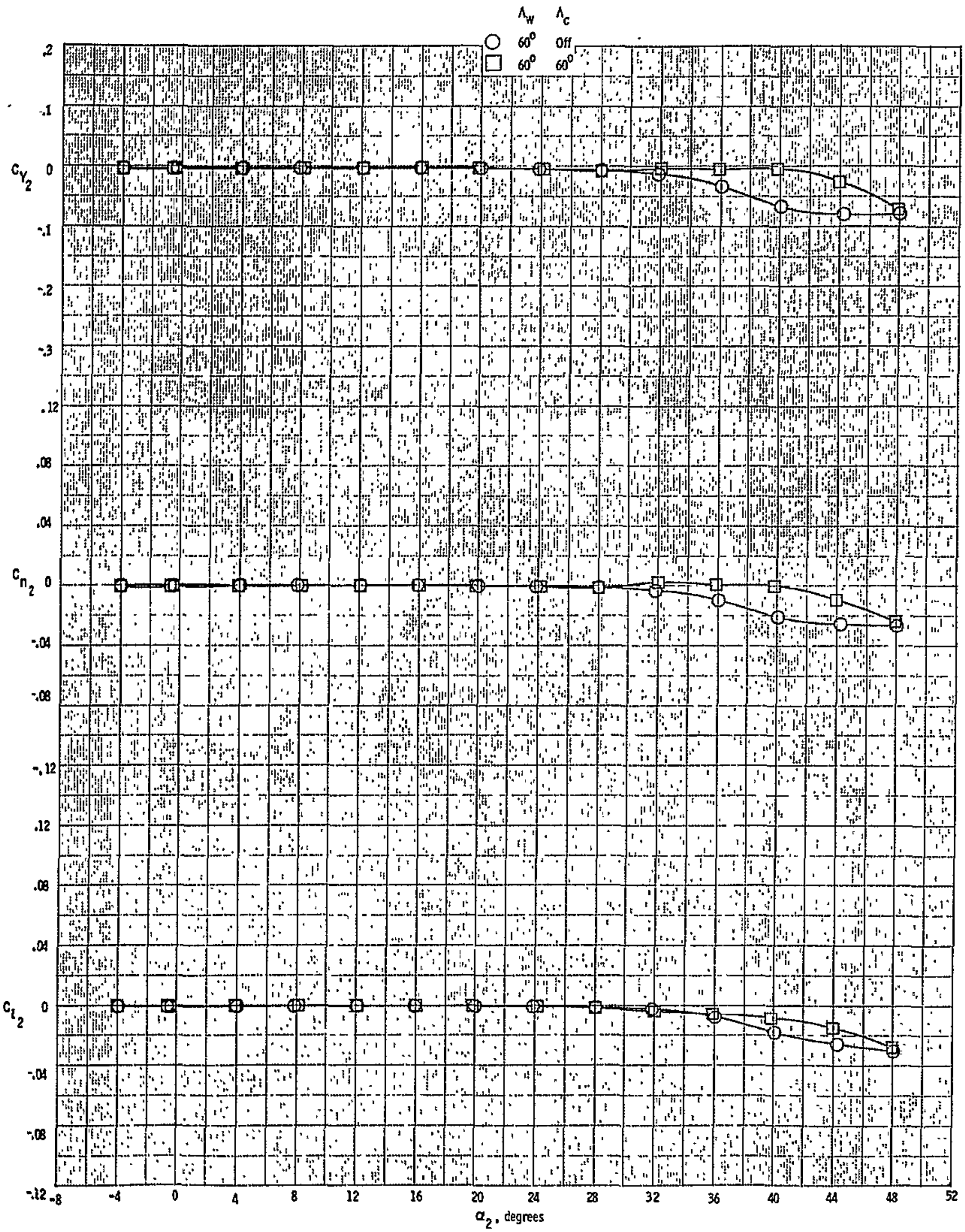


(d) Nose balance lateral-directional data
Figure 4. Concluded.

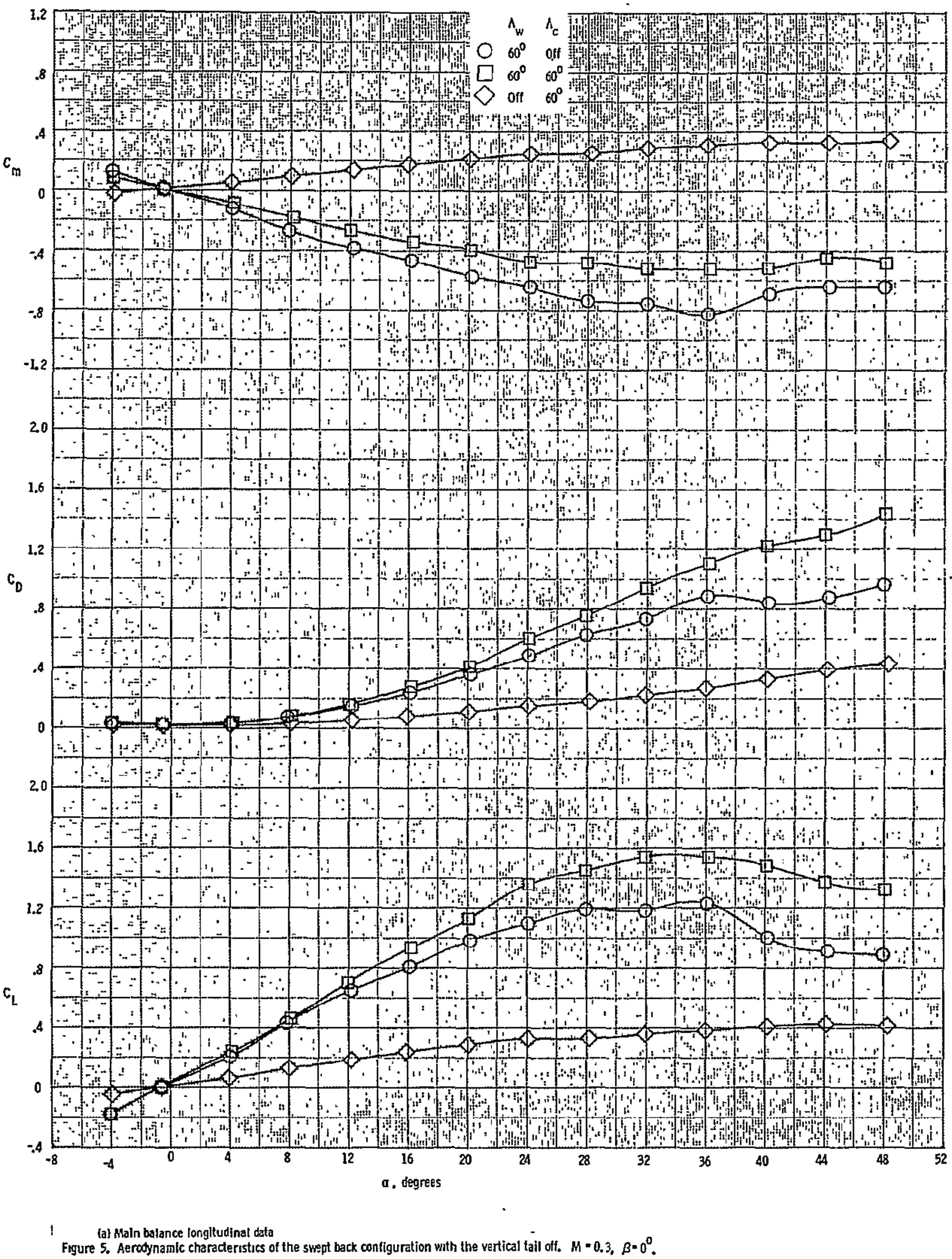


(a) Main balance longitudinal data

Figure 5. Aerodynamic characteristics of the swept back configuration with the vertical tail off. $M = 0.3$, $\beta = 0^\circ$.

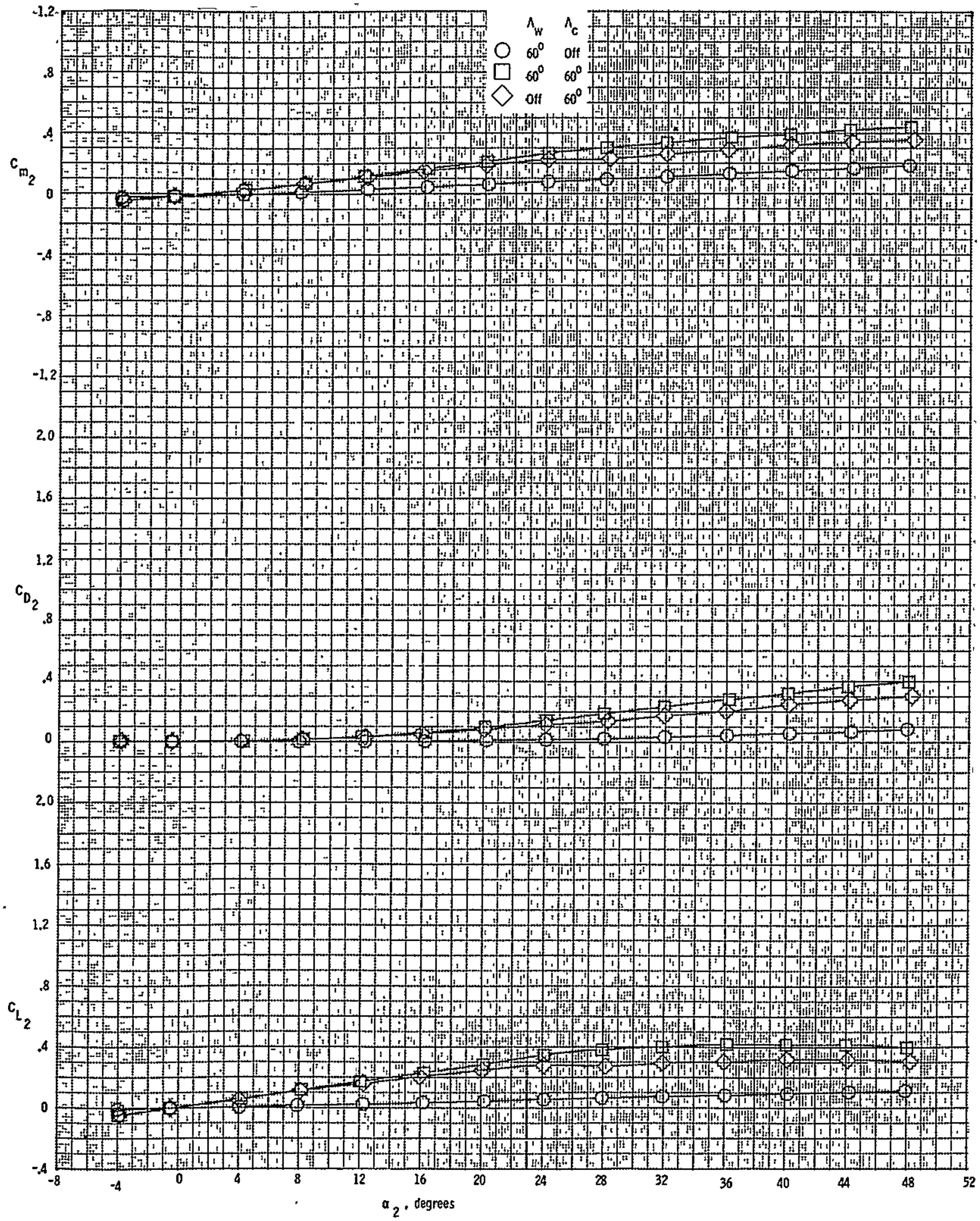


(b) Nose balance longitudinal data
Figure 5. Continued.

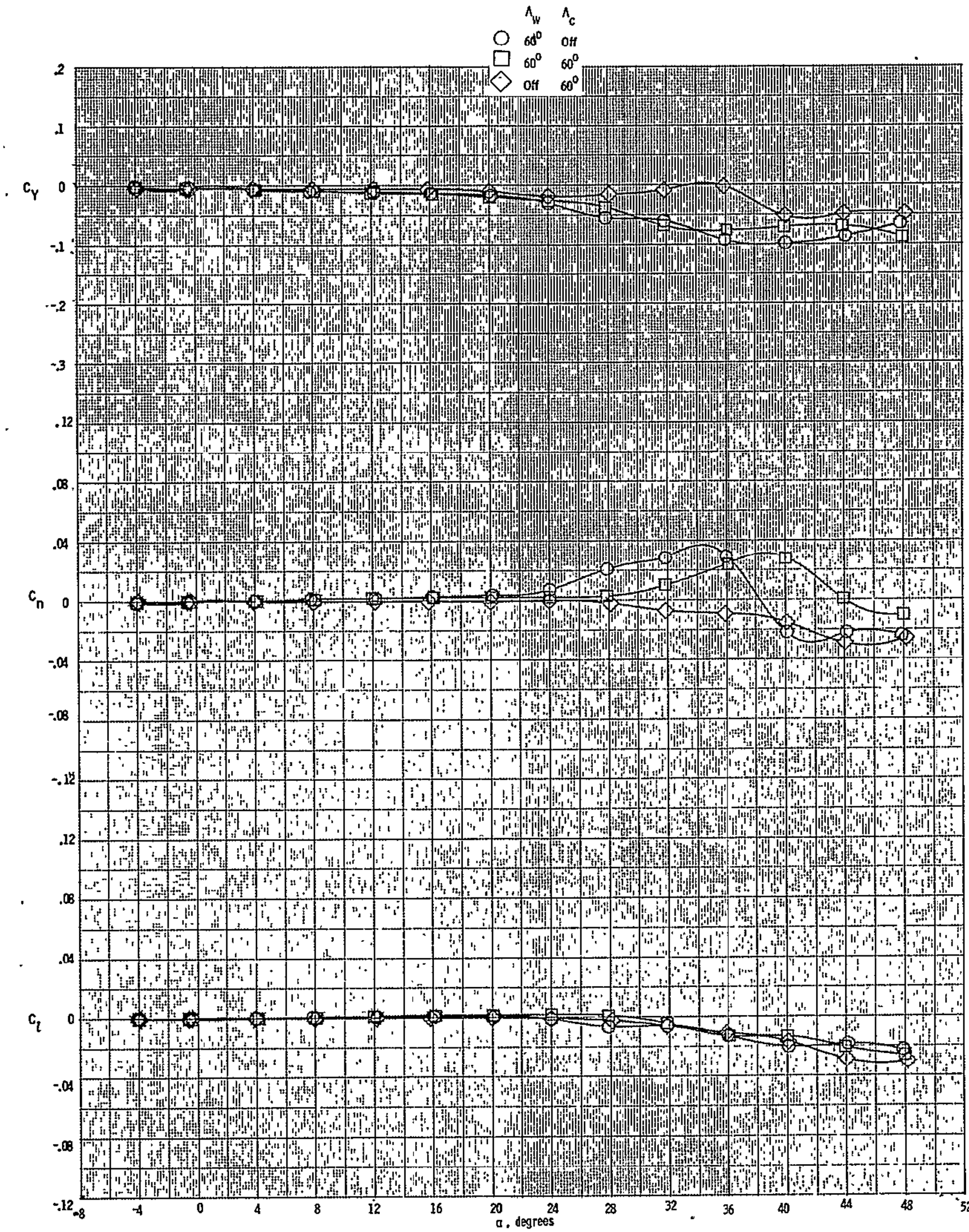


(c) Main balance lateral-directional data

Figure 5. Continued.

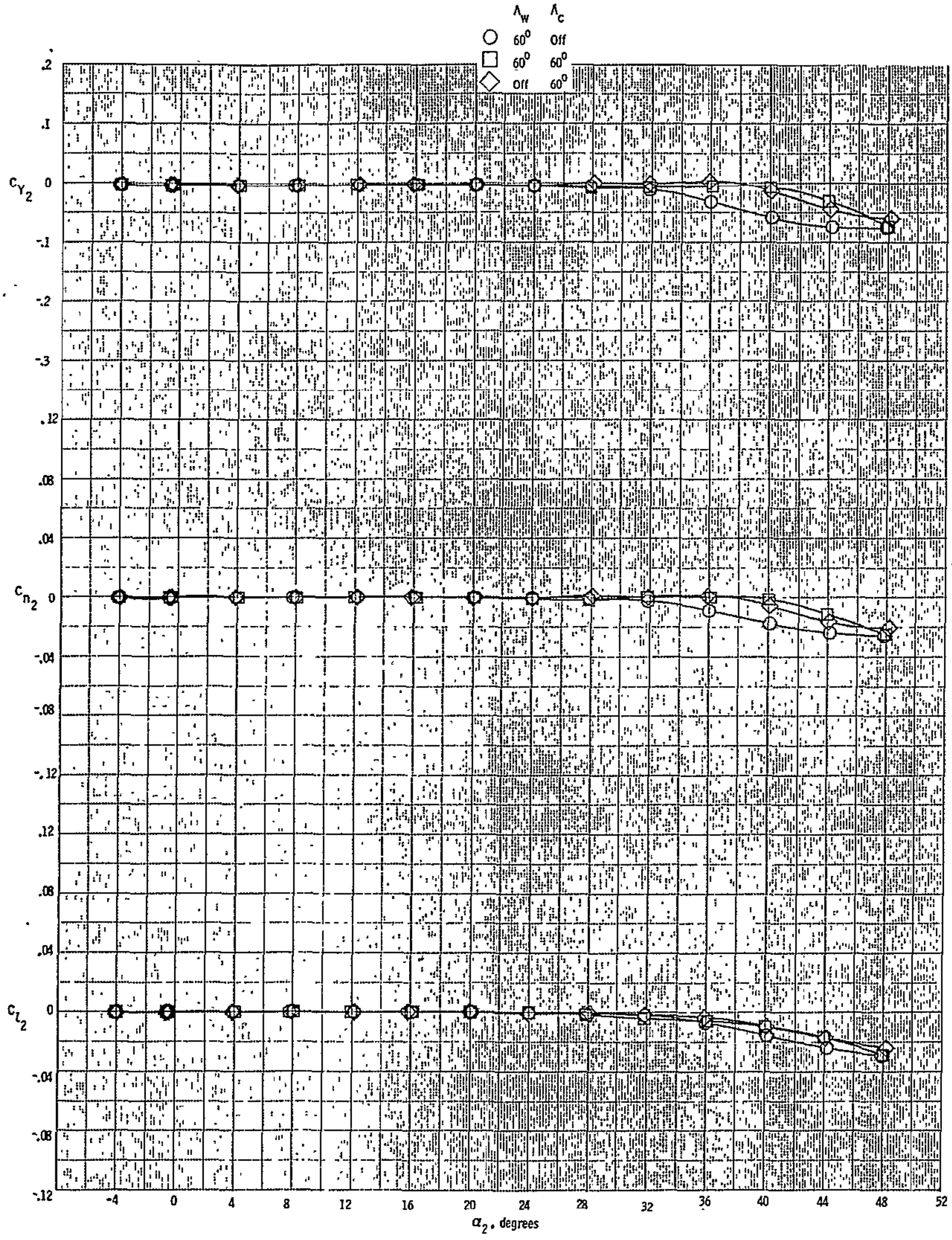


(d) Nose balance lateral-directional data

Figure 5. Concluded.

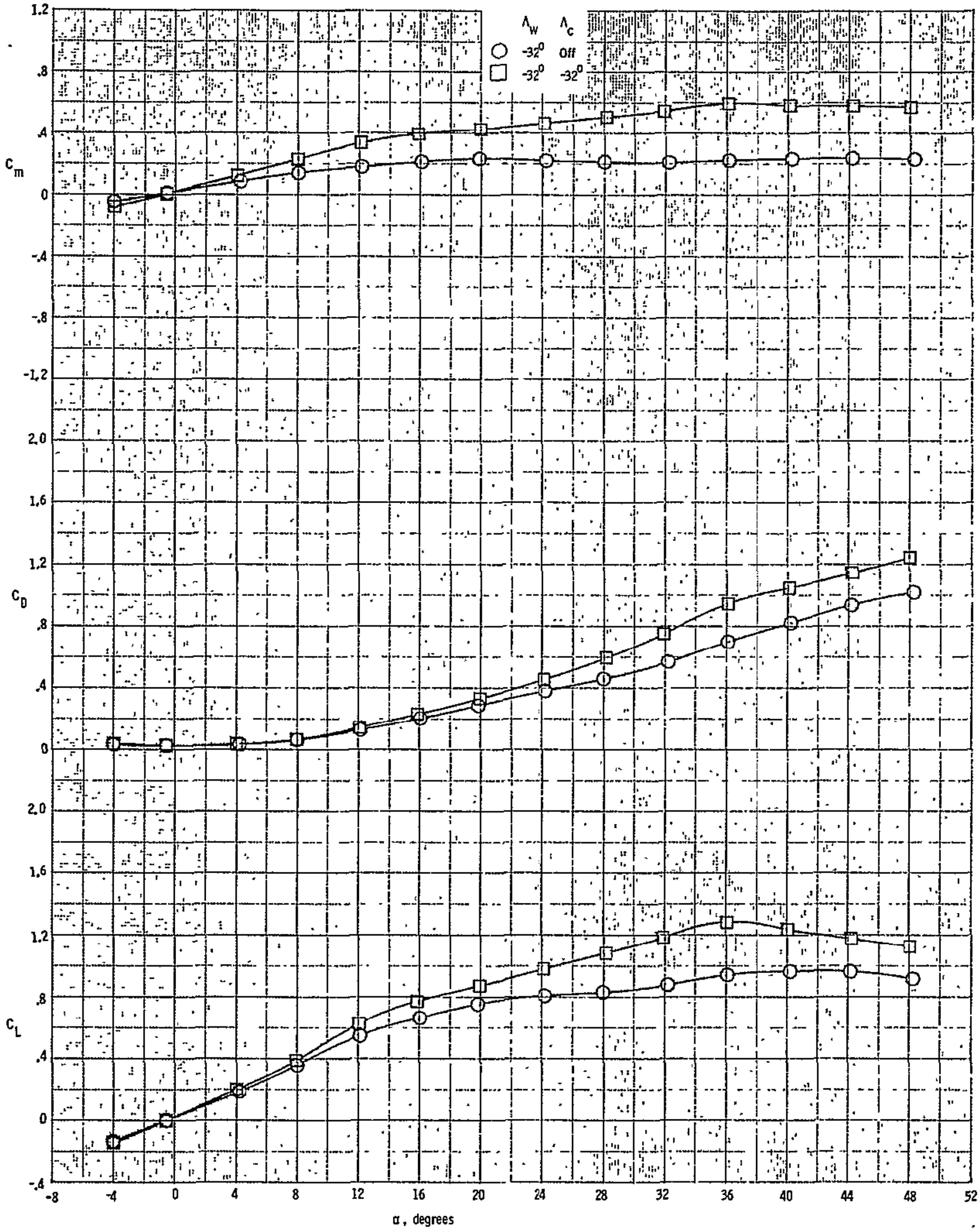


(a) Main balance longitudinal data

Figure 6. Aerodynamic characteristics of the swept forward configuration with the vertical tail on. $M = 0.3$, $\beta = 0°$.

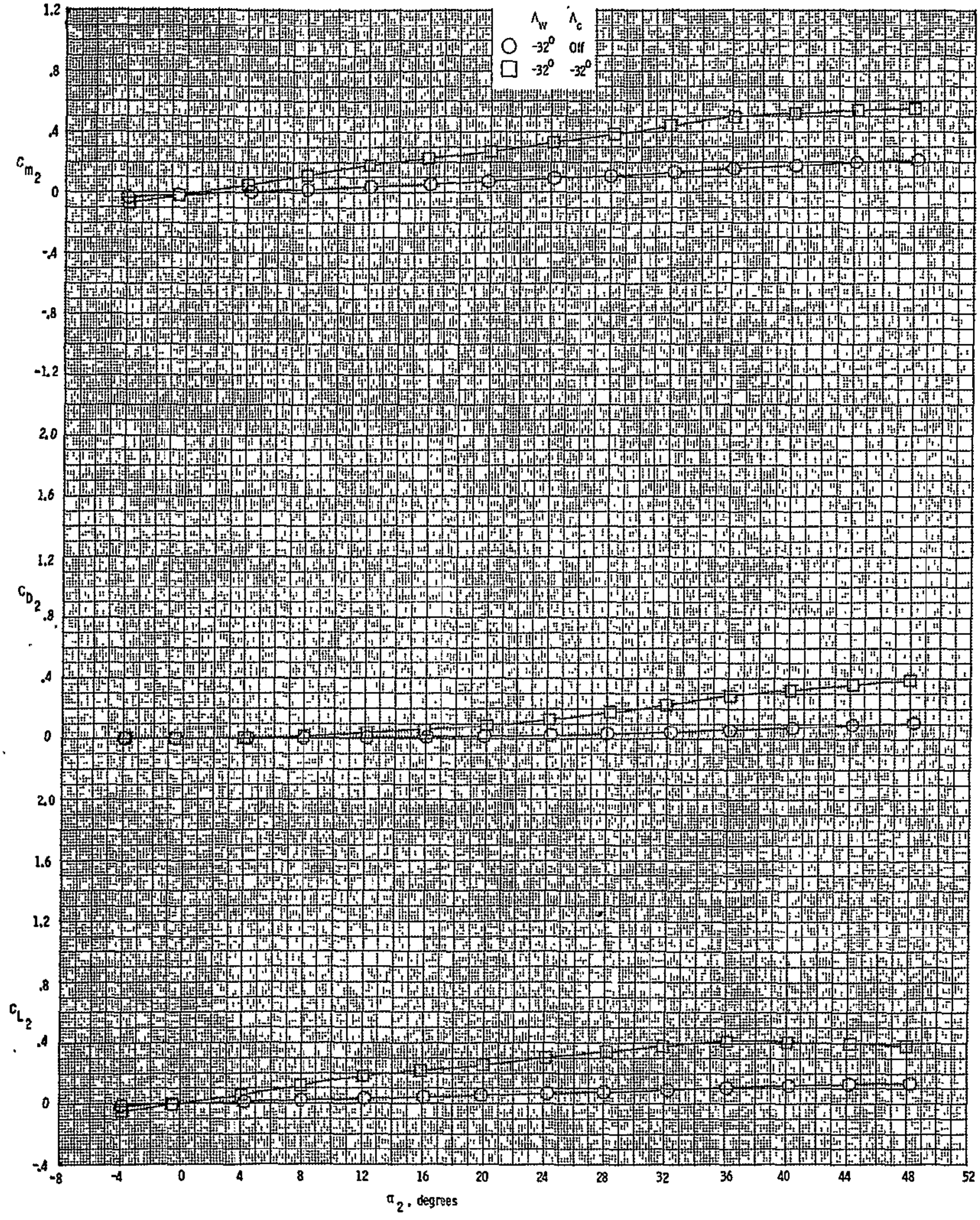


(b) Nose balance longitudinal data

Figure 6. Continued.

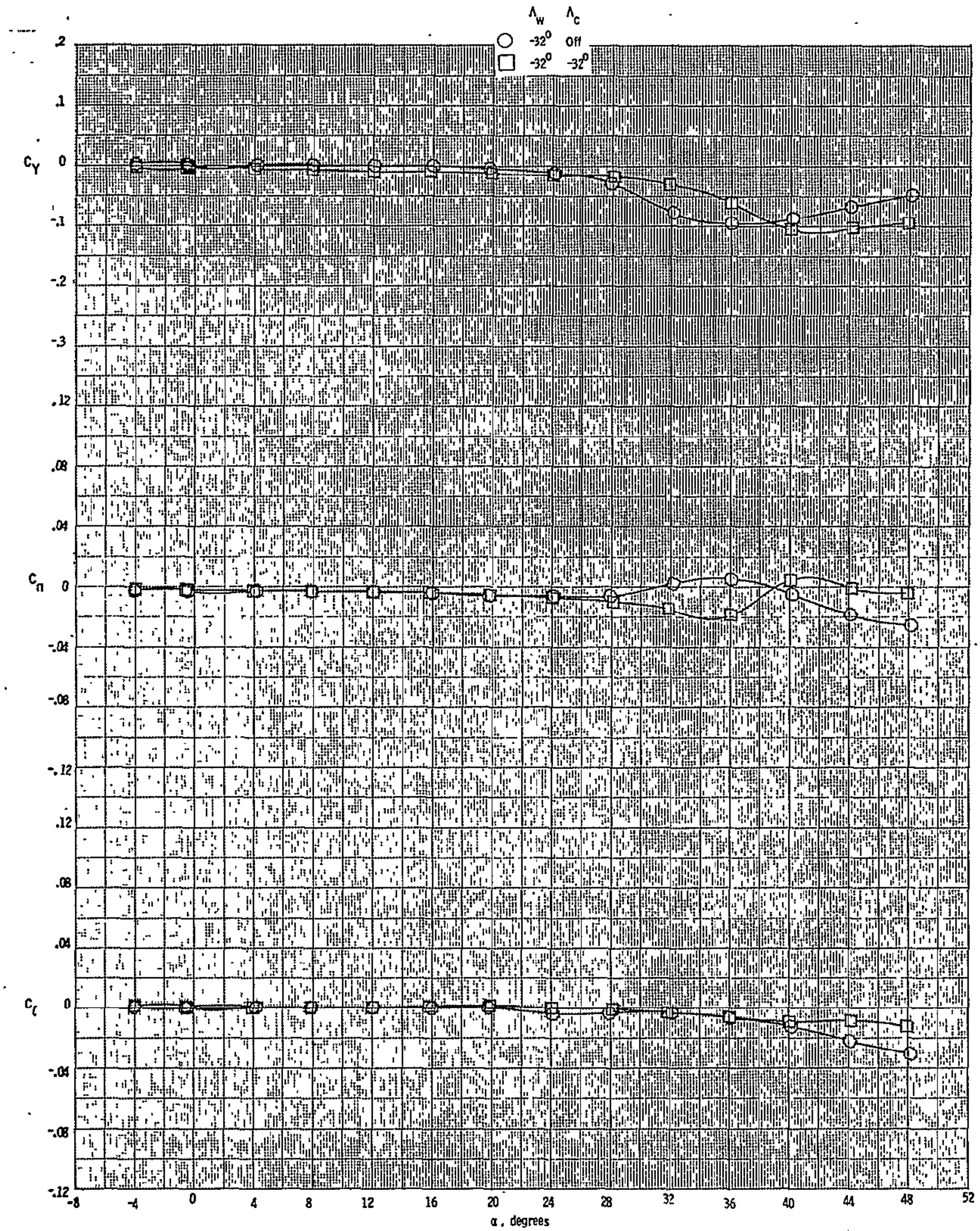


(c) Main balance lateral-directional data.

Figure 6. Continued.

ORIGINAL PAGE IS
OF POOR QUALITY

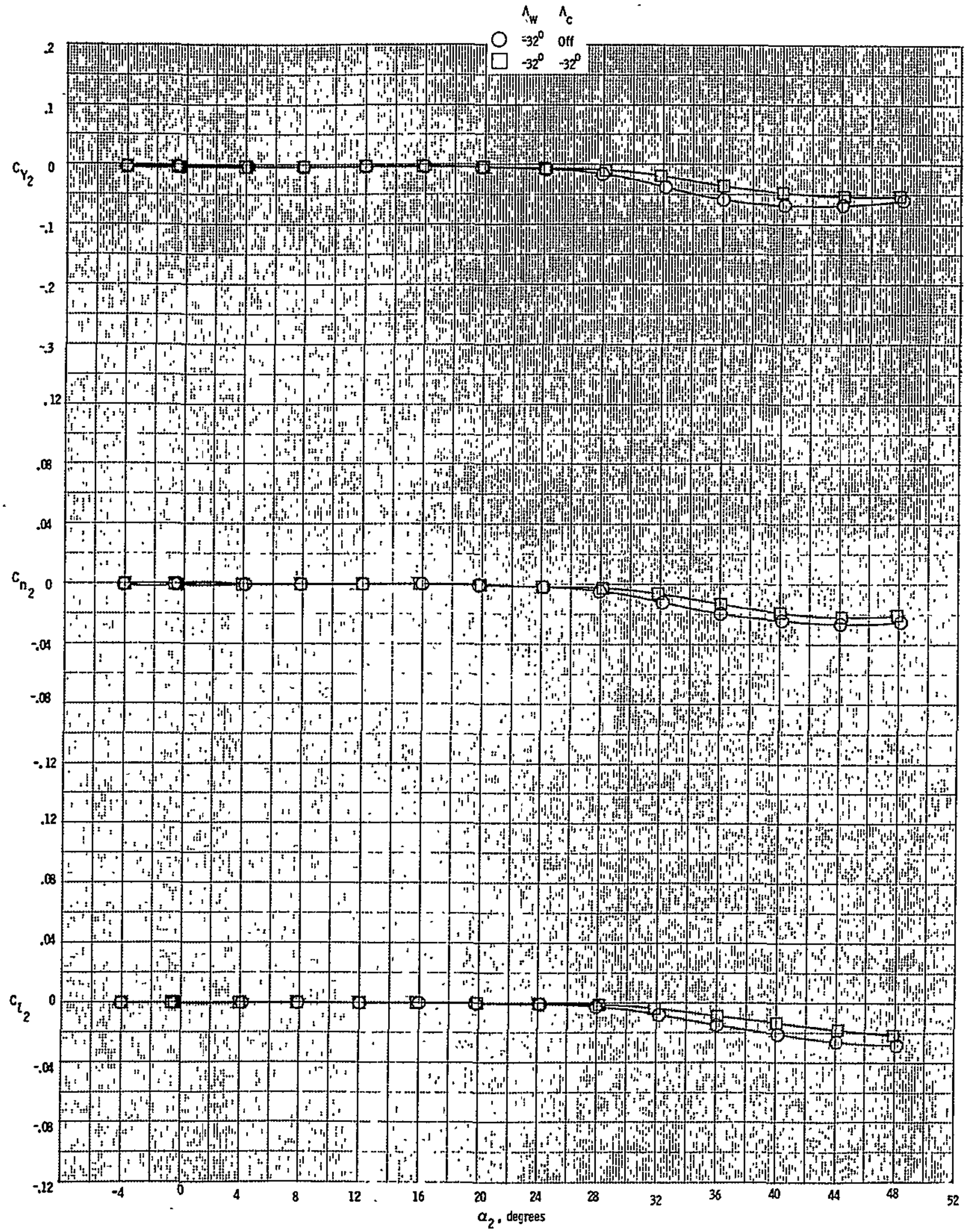


(d) Nose balance lateral-directional data
Figure 6. Concluded.

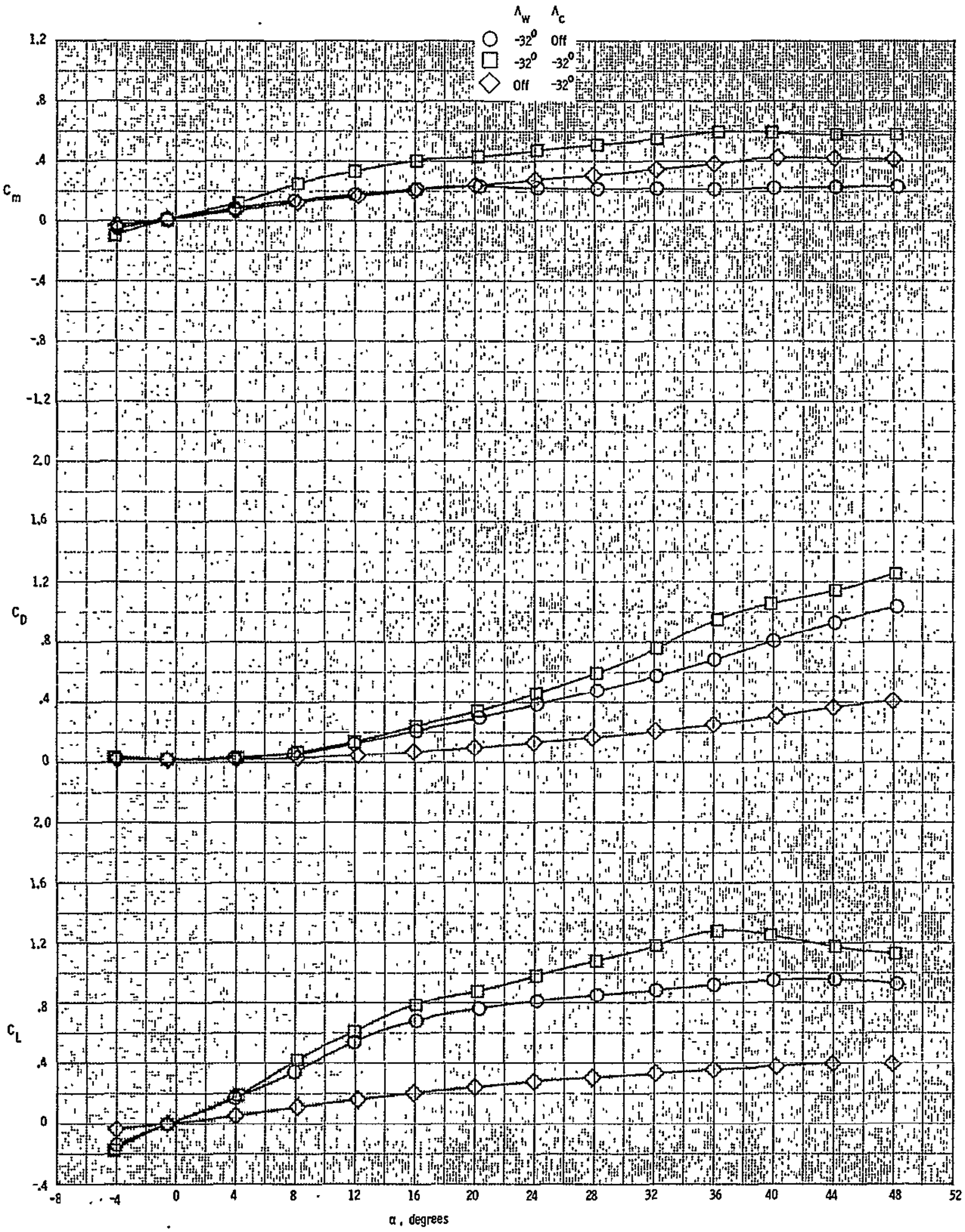


(a) Main balance longitudinal data

Figure 7. Aerodynamic characteristics of the swept forward configuration with the vertical tail off. $M = 0.3$, $\beta = 0^\circ$.

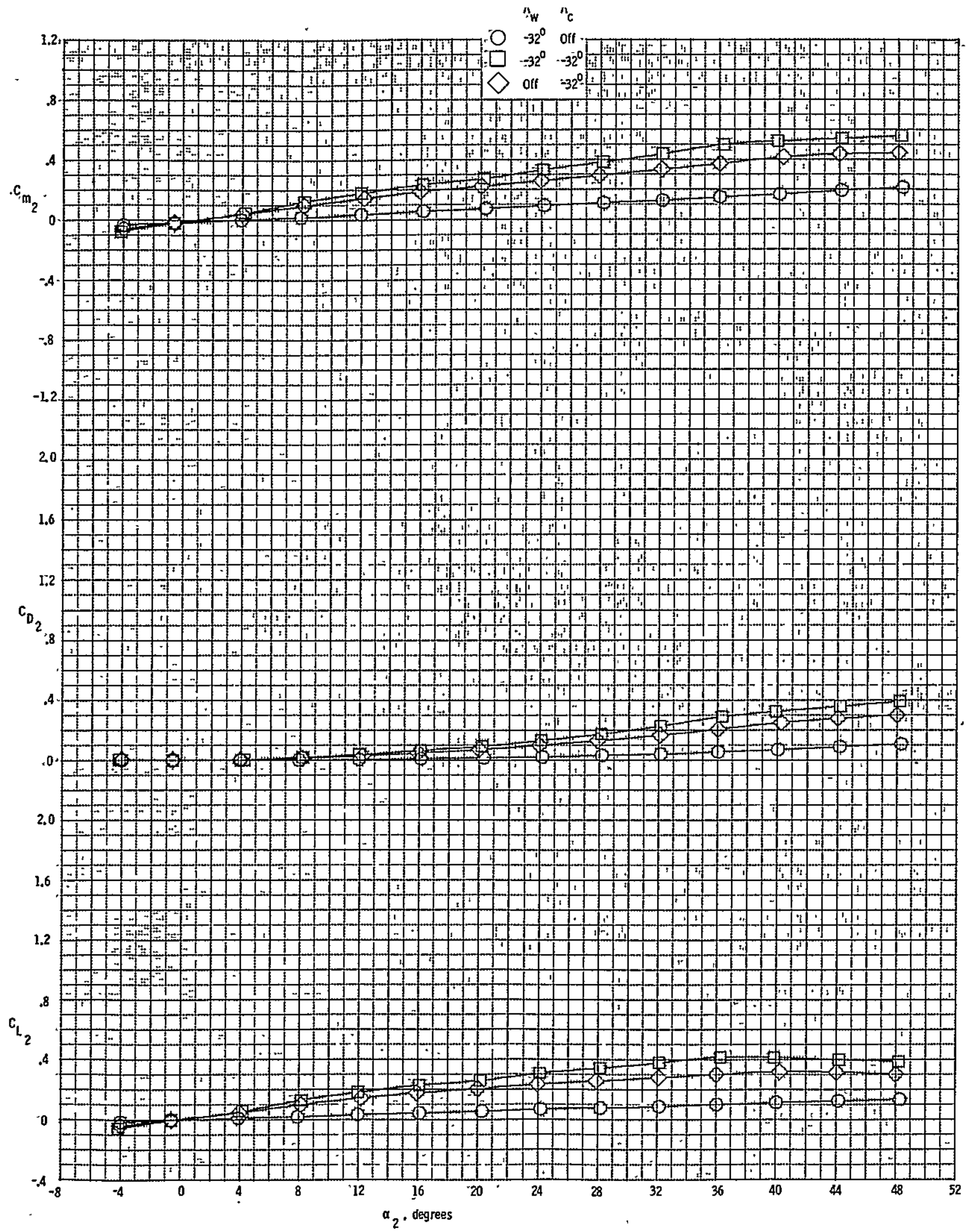


(b) Nose balance longitudinal data
Figure 7. Continued.

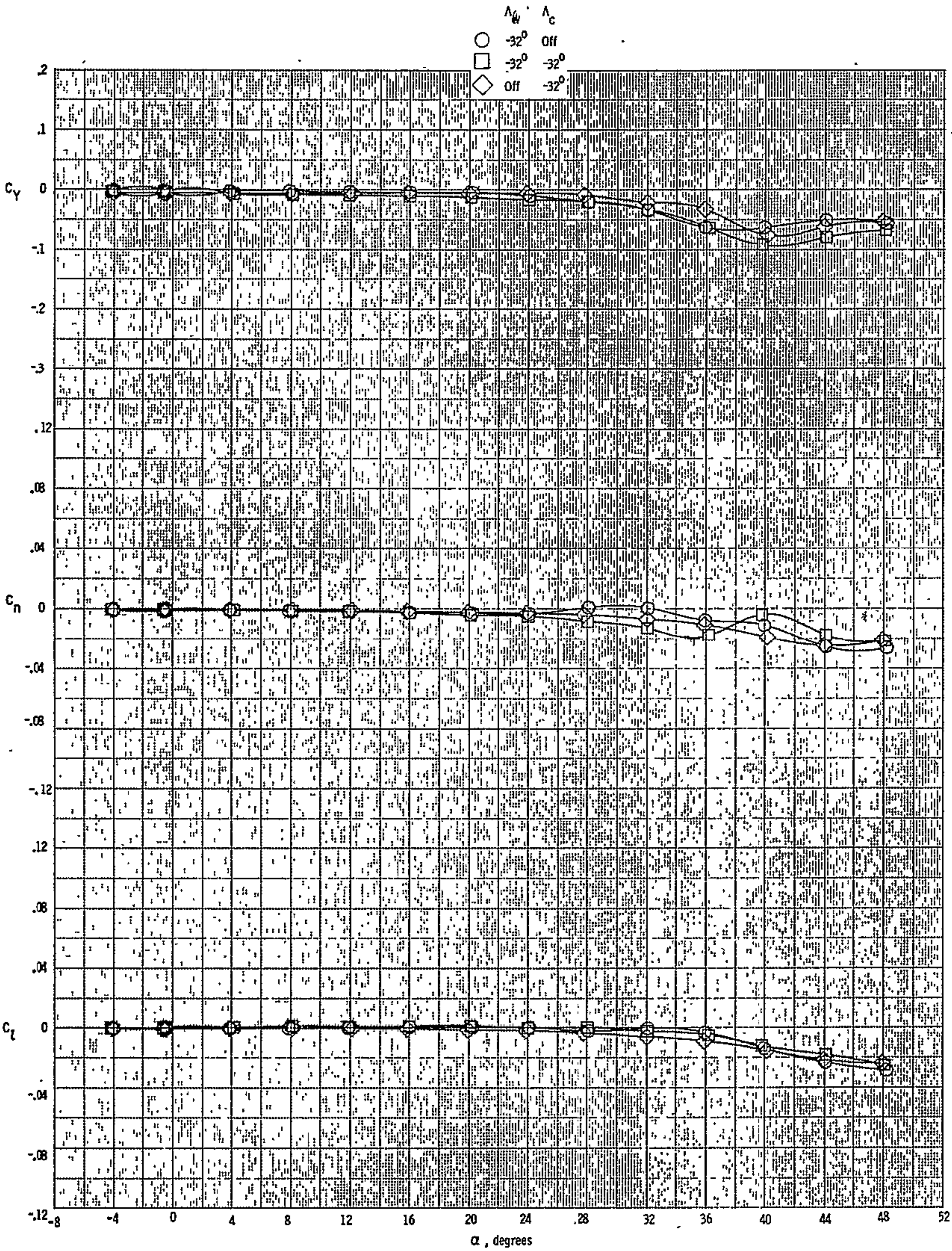


(c) Main balance lateral-directional data
Figure 7. Continued.

ORIGINAL PAGE IS
OF POOR QUALITY

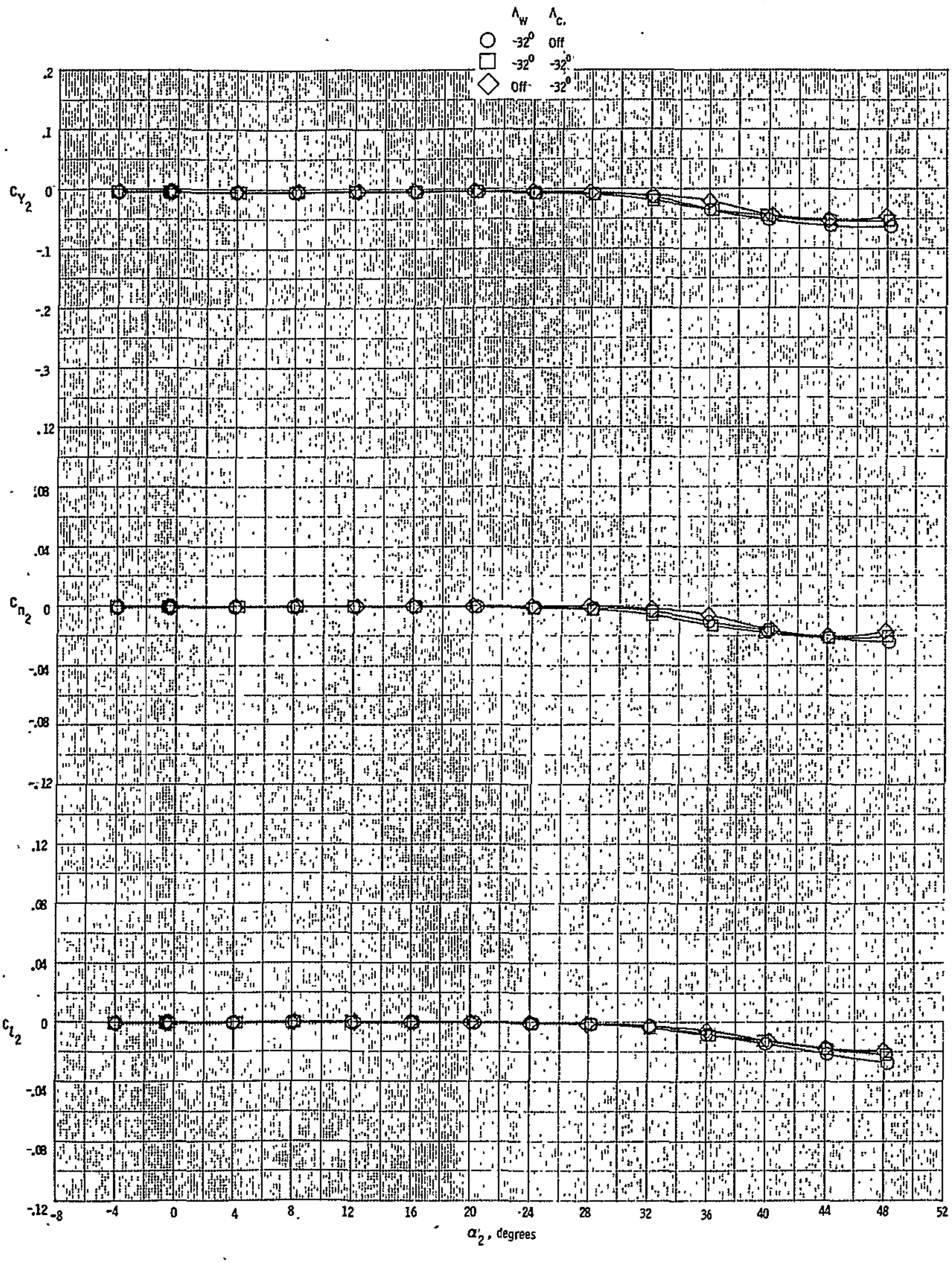


(d) Nose balance lateral-directional data
Figure 7. Concluded.

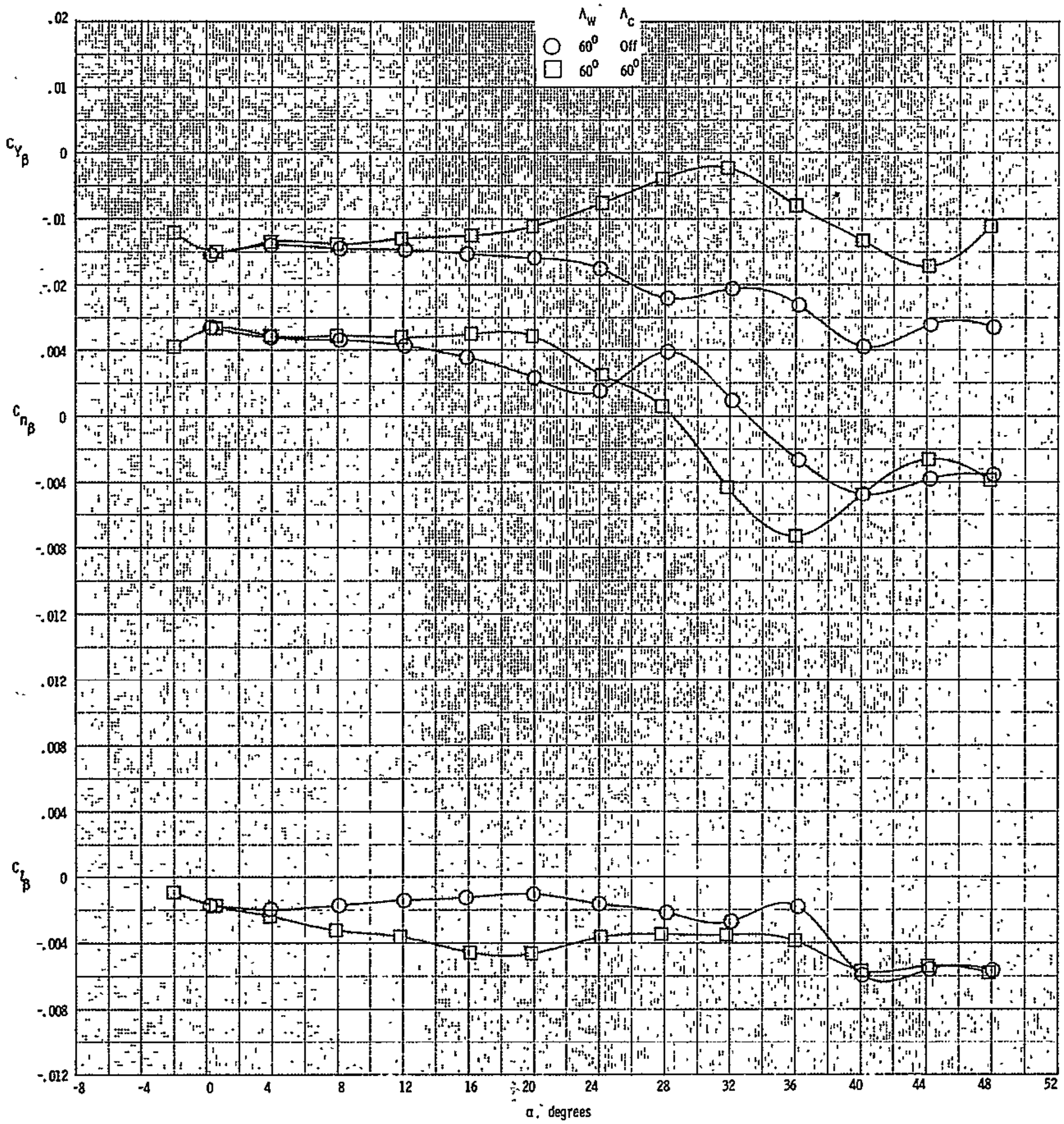


(a) Main balance data.

Figure 8. - Lateral-directional aerodynamic stability derivative characteristics of the swept back configuration with vertical tail on. M = 0.3.

ORIGINAL PAGE IS
OF POOR QUALITY

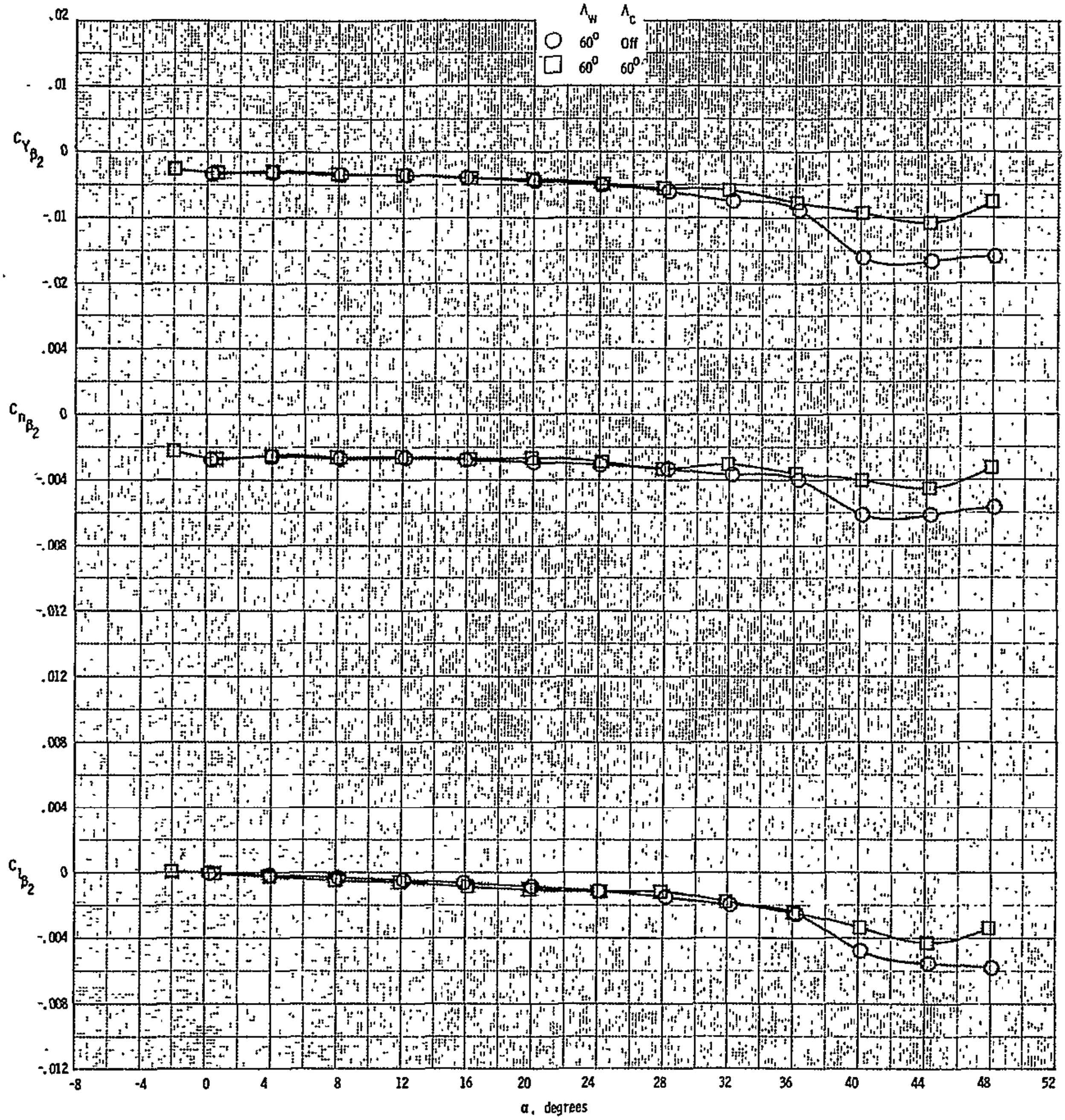


(b) Nose balance data.

Figure 8. - Concluded.

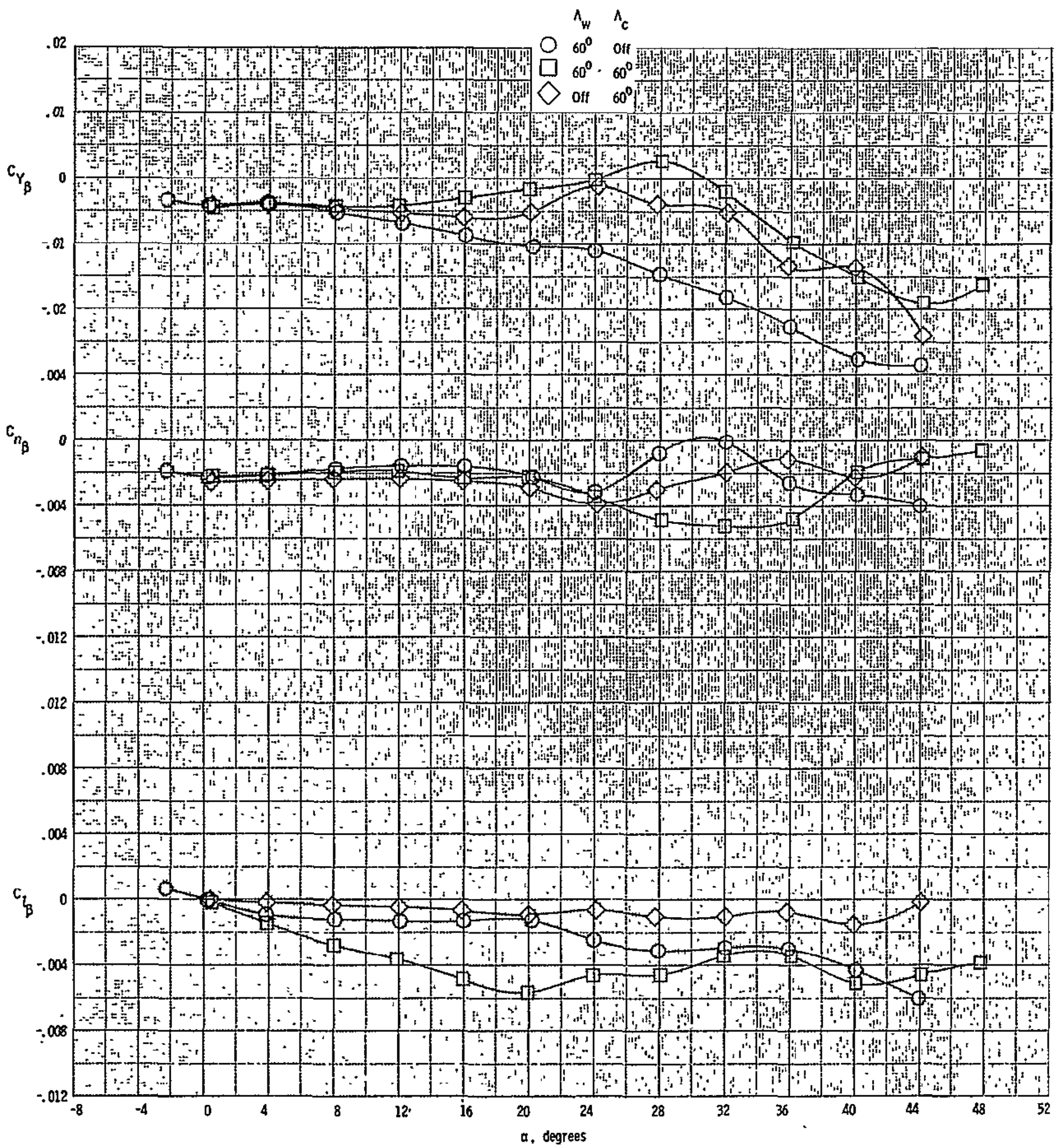


(a) Main balance data

Figure 9. - Lateral-directional aerodynamic stability derivative characteristics of the swept back configuration with vertical tail off. M = 0.3.

ORIGINAL PAGE IS
OF POOR QUALITY

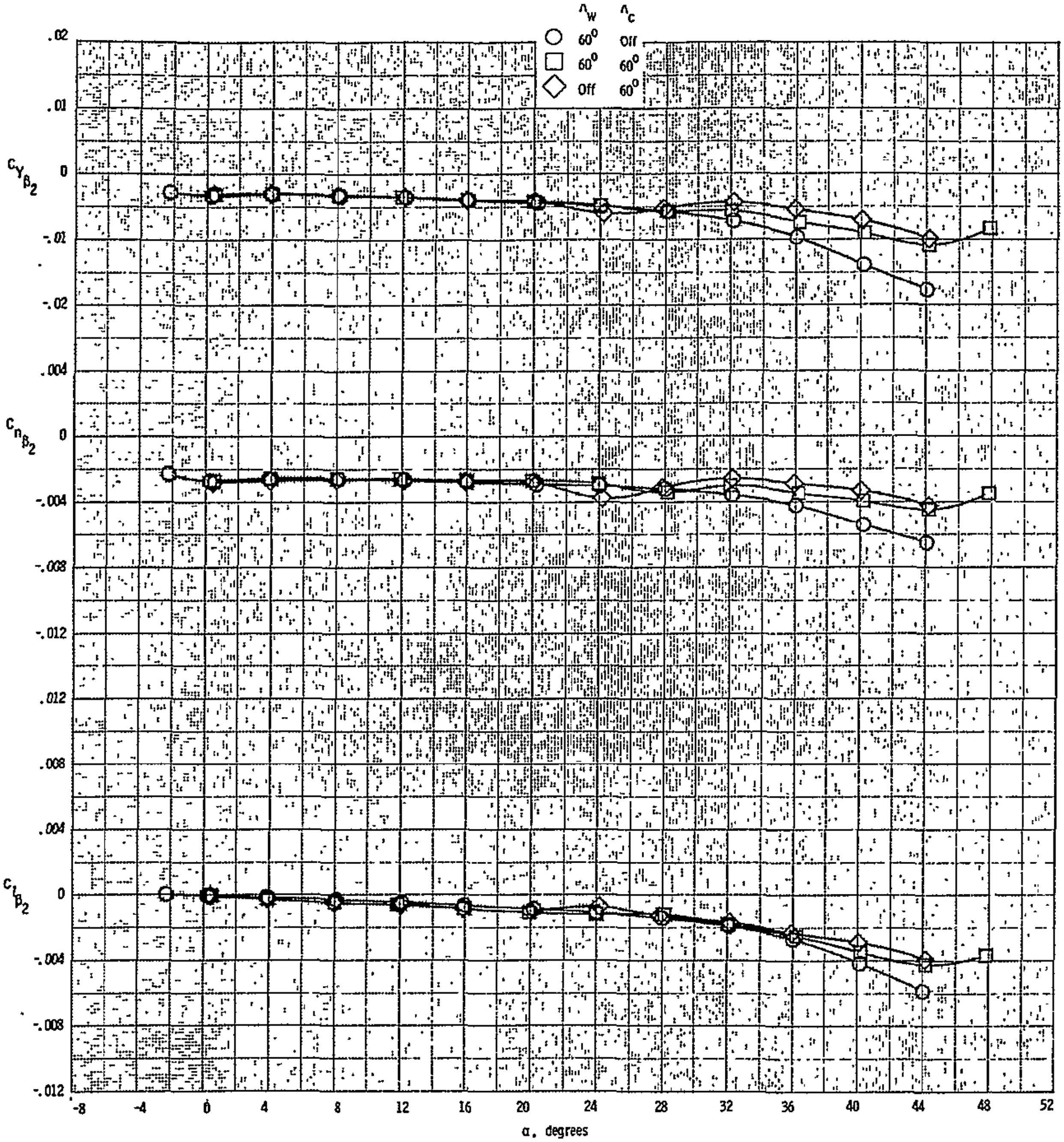


(b) Nose balance data.

Figure 9. - Concluded.

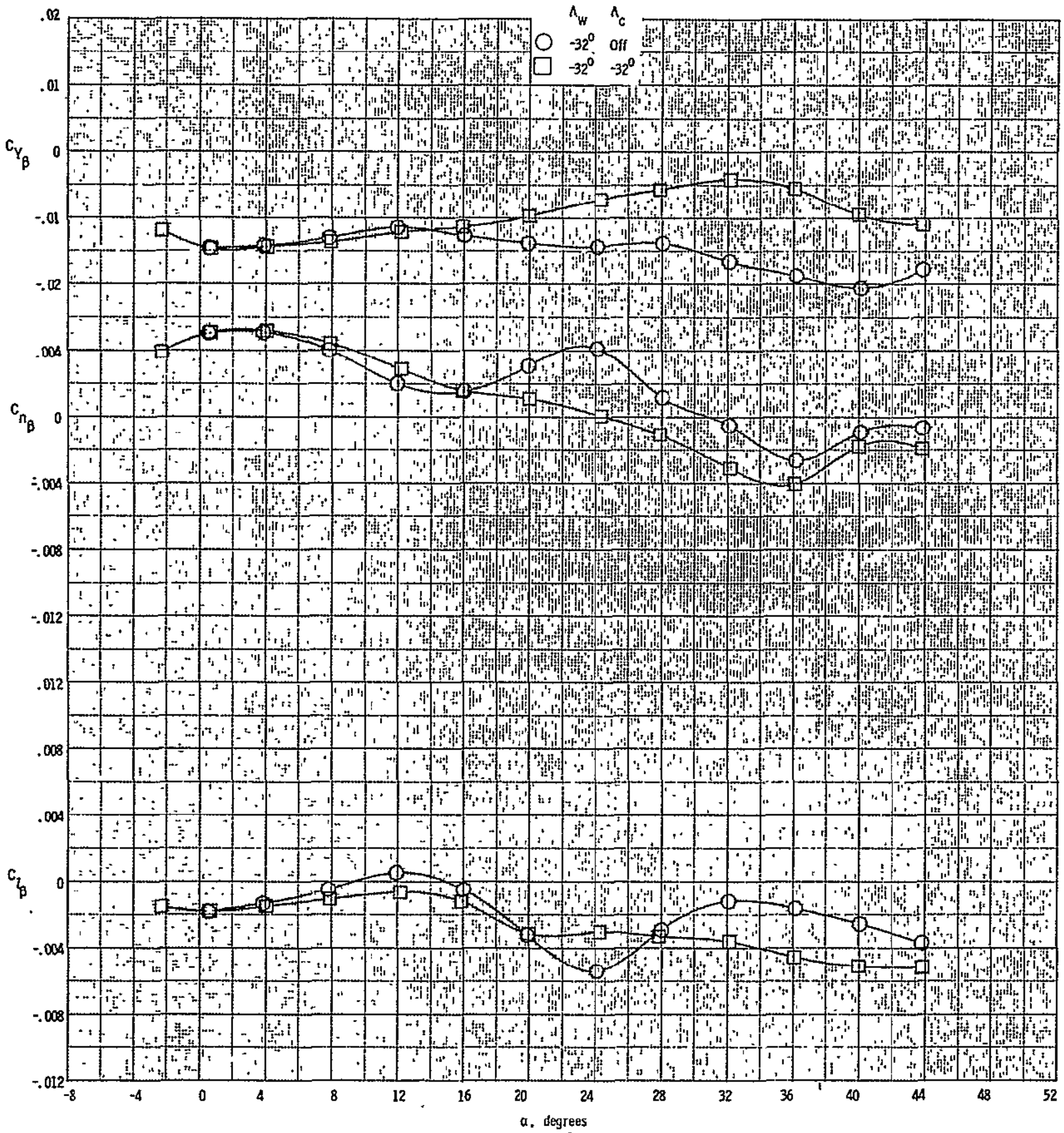


(a) Main balance data.

Figure 10. - Lateral-directional aerodynamic stability derivative characteristics of the swept forward configuration with vertical tail on. M = 0.3.

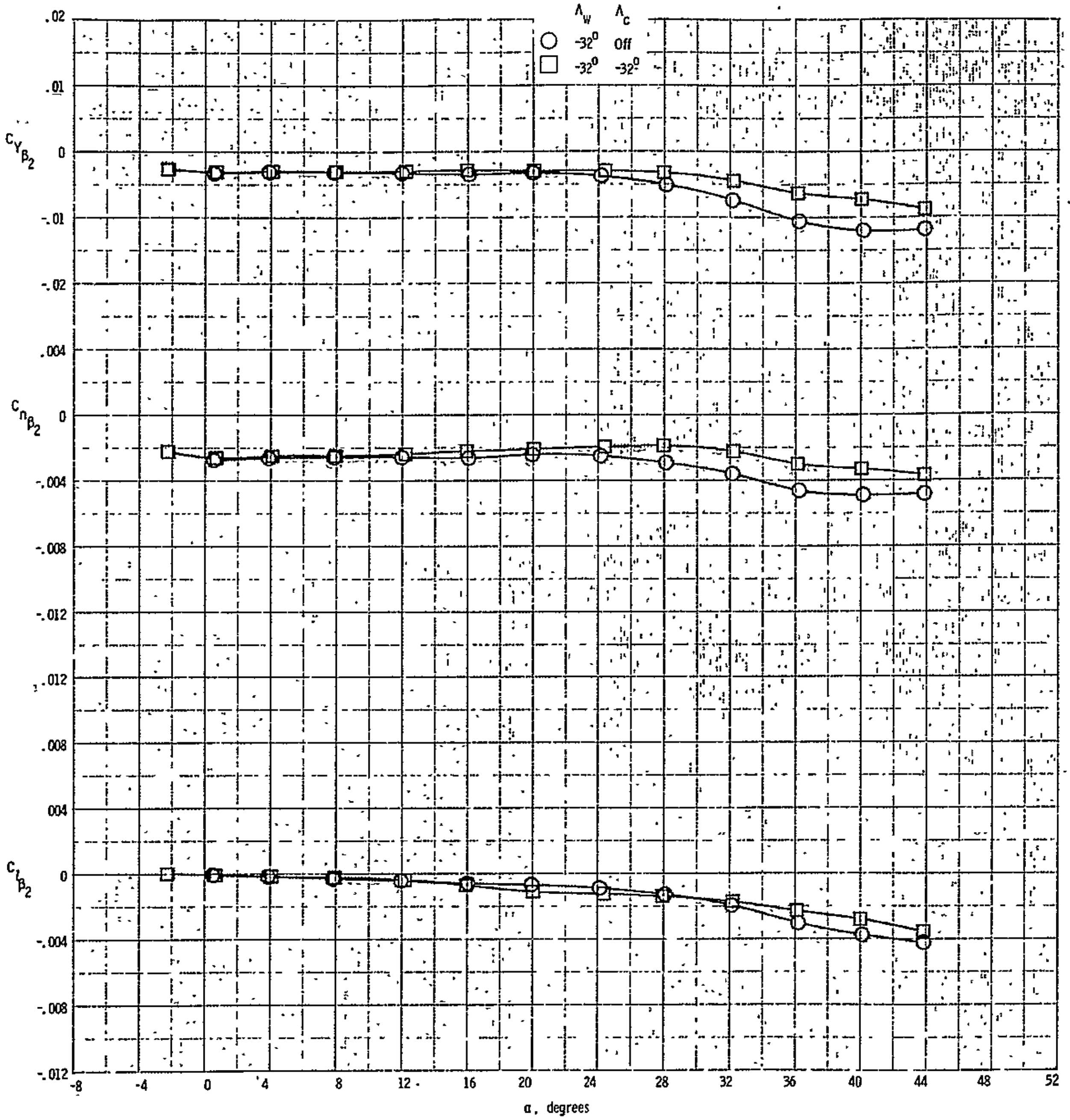


(b) Nose balance data.

Figure 10.- Concluded.

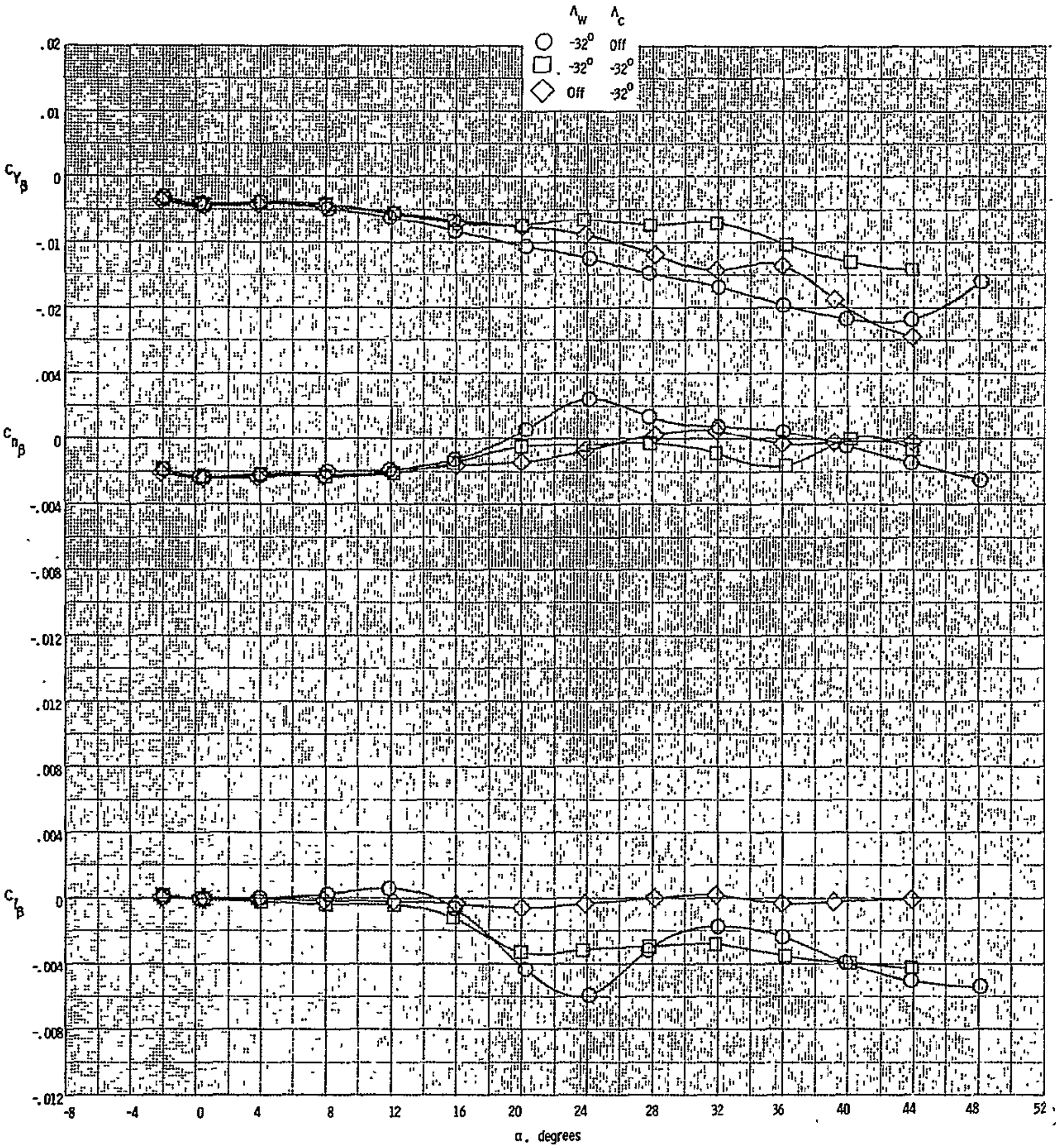


(a) Main balance data.

Figure 11.- Lateral-directional aerodynamic stability derivative characteristics of the swept forward configuration with vertical tail off. $M = 0.3$

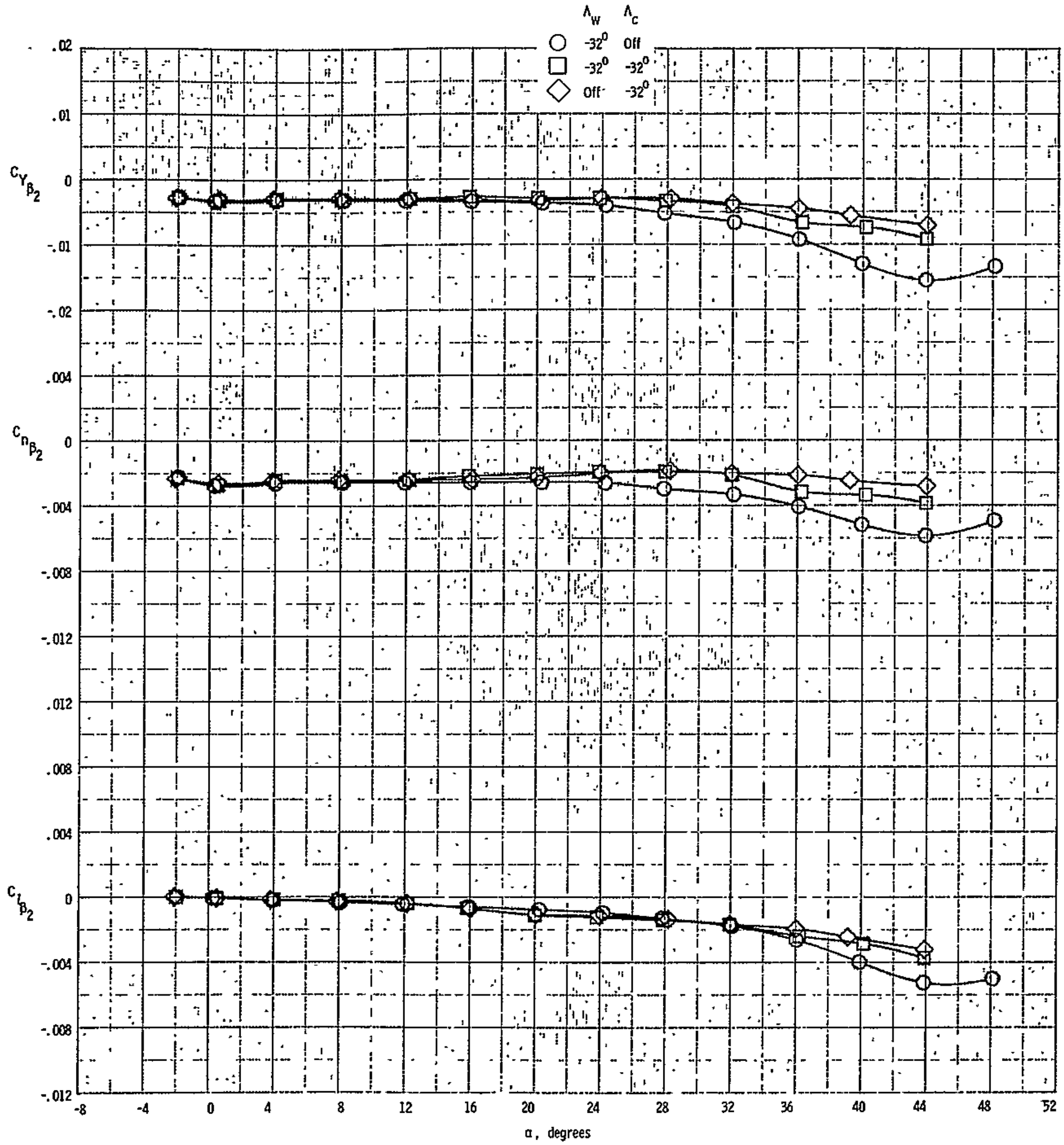


(b) Nose balance data.

Figure 11 - Concluded.

| 1. Report No. | 2. Government Accession No. | 3. Recipient's Catalog No. |
|---|---|---|
| NASA TM 74092 | | |

| 4. Title and Subtitle | 5. Report Date |
|---|---|
| SUBSONIC LONGITUDINAL AND LATERAL-DIRECTIONAL STATIC AERODYNAMIC CHARACTERISTICS FOR A CLOSE-COUPLED WING-CANARD MODEL IN BOTH SWEPT BACK AND SWEPT FORWARD CONFIGURATIONS | February 1978 |
| | 6. Performing Organization Code: 3850 |
| 7. Author(s): Jarrett K. Huffman and Charles H. Fox, Jr. | 8. Performing Organization Report No. |
| | 10. Work Unit No. |
| 9. Performing Organization Name and Address: NASA Langley Research Center, Hampton, Virginia 23665 | 11. Contract or Grant No. |
| | 13. Type of Report and Period Covered: Technical Memorandum |
| 12. Sponsoring Agency Name and Address: National Aeronautics and Space Administration, Washington, DC 20546 | 14. Sponsoring Agency Code |

15. Supplementary Notes

16. Abstract


A general research fighter model was tested in the Langley 7- by 10-foot high speed tunnel at a Mach number of 0.3. The close-coupled wing-canard combination was tested with both lifting surfaces in a $60^{\circ}$ swept back configuration and in a $32^{\circ}$ swept forward configuration. The angle-of-attack range was from approximately $-4^{\circ}$ to $48^{\circ}$ at sideslip angles of $0^{\circ}$, $-5^{\circ}$, and $5^{\circ}$. The data are presented without analysis in order to expedite publication.


| 17. Key Words (Suggested by Author(s)) | 18. Distribution Statement |
|---|---|
| Longitudinal aerodynamics<br>Lateral-directional aerodynamics<br>Close-coupled wing-canard<br>Swept forward wing-canard<br>Subsonic aerodynamics | Star Category - 02<br><br>Unclassified - Unlimited |

| 19. Security Classif. (of this report) | 20. Security Classif. (of this page) | 21. No. of Pages | 22. Price* |
|---|---|---|---|
| Unclassified | Unclassified | 58 | $4.50 |

* For sale by the National Technical Information Service, Springfield, Virginia 22161